A THEORETICAL AND EXPERIMENTAL STUDY OF RADIATION DAMAGE IN DRIFT-FIELD SOLAR CELLS

PRINCETON RESEARCH & DEVELOPMENT CO.
CHERRY VALLEY ROAD
PRINCETON, NEW JERSEY

A THEORETICAL AND EXPERIMENTAL STUDY OF RADIATION DAMAGE IN DRIFT-FIELD SOLAR CELLS

Annual Report
Contract NAS5-9580
Date: May 10, 1966

Submitted to:

NASA-Goddard Space Flight Center
Greenbelt, Maryland

Prepared by:

J. A. Baicker
Princeton Research & Development Co.
Box 641
Princeton, N.J.

I. SUMMARY

28417

This report describes the results of a theoretical and experimental study of drift field solar cells. The objective of the program was a general comparison of drift field cells with conventional solar cells, and in particular to understand and to predict the radiation damage behavior of drift field cells.

The work which is reported here concentrates on two specific investigations: the current-voltage relationships in drift field cells compared with conventional cells; and the spectral response of the two types of cell. In both phases of the program detailed measurements were carried out at various sample temperatures, and in normal and irradiated cells. The temperatures were in the range from room temperature down to 77°K, and the irradiations were with 1 MeV electrons and 3 MeV protons.

The results of the investigations provide clear indications of the reasons for the failure of drift field cells to outlast conventional cells when they are operated in a radiation environment.

II. CURRENT-VOLTAGE CHARACTERISTICS

A conventional silicon solar cell is very nearly a classical abrupt p-n junction with perfect planar geometry. The base region has a uniform, homogeneous concentration of impurities (donors or acceptors, depending on the conductivity type). The surface layer has a large gradient in impurity concentration, but this is of little practical importance. The transition between surface and base regions is well-defined, and consequently the depletion layer is quite narrow (much less than 1 micron thick).

In a device of this description, the currents which flow under both forward and reverse bias conditions can be attributed to several sources. One source is a diffusion current consisting of minority carriers which diffuse into the depletion layer and are then swept across the junction by the internal electric field within the depletion layer and any external bias which may be applied. At zero external bias the total net current flow is zero, and this condition is achieved by a detailed balance between minority carriers flowing across the junction and generation-recombination on both sides of the junction.

In addition to the diffusion current, there is also a current produced by thermal generation-recombination within the depletion layer. The features of the generation-recombination current have been treated by Sah, Noyce, and Shockley[1].

In the work which is described in this report, we have confined most of our observations to low current-voltage conditions. By this we mean that the injected current in the forward direction does not produce non-equilibrium carrier concentrations that are comparable to the majority carrier concentration in the lighter-doped side of the junction, and that the applied bias in the reverse direction is not large compared with the electrostatic potential barrier at the junction. Under these conditions,

the thermal diffusion current should have a voltage dependence that is given by the ideal diode equation

$$I = I_o\left[\exp\left(qV/kT\right) - 1\right] \qquad (1)$$

According to this equation, the forward current goes approximately as exp(qV/kT) and the reverse current saturates at a value of I_o.

The thermal diffusion current at intermediate current levels approaches a voltage dependence that is given by exp(qV/2kT).

The space-charge region generation-recombination current[1] should go as exp(qV/2kT) in the forward direction and as V^n in the reverse direction, where n is between 1/3 and 1/2 depending on the shape of the impurity profile in the vicinity of the junction (i.e., whether the junction is gradual or abrupt).

Both of the currents discussed above have characteristic voltage and temperature dependence. In addition to these currents several other types of currents are observed. The most important of these is a current in the forward direction which has a much slower voltage dependence than either of the previous cases. In some of the individual cells we have studied, notably the early drift field cells, this component manifests itself strongly at low and intermediate forward biases.

We have termed this current the "excess current" following the nomenclature used to describe similar currents in tunnel diodes.

Under large forward or reverse bias conditions there are effects other than those described above. Large forward currents are accompanied by series resistance effects, and large reverse biases produce leakage currents which may exceed I_o. The I-V characteristics as described can be analyzed using the equivalent circuit shown in Fig. 1.

So far we have confined our discussion to an idealized conventional solar cell. Extending it to drift field cells imposes no major changes in the phenomena to be expected. Currents which originate in the space charge region should be essentially

the same as for conventional cells, at least in the forward direction. In the reverse direction the space charge g-r current will differ only slightly in the two cases. The thermal current in the forward direction consists mainly of majority carriers from the surface layer which are injected into the base. Since there is not any special difference between surface layer production methods in conventional vs. drift field cells the thermal currents are expected to be the same.

Temperature Effects

The temperature dependence of the I-V characteristics can be qualitatively deduced from our previous discussion. The thermal current has a voltage dependence that is strongly temperature-dependent; at low temperature the current is more steeply voltage dependent than at high temperature. In addition, I_o decreases rapidly with decreasing temperature. If we are observing a minority carrier diffusion current, I_o will have a temperature dependence that is given approximately by $\exp(-E_g/kT)$ neglecting factors which are only slightly temperature-dependent. In this expression, E_g is the bandgap energy.

If I_o is due to g-r current in the space charge region its temperature dependence depends on the location of the g-r centers in the band gap. For centers lying midway between valence and conduction bands the temperature dependence is given approximately by $\exp(-E_g/2kT)$.

We are unable to deduce the temperature dependence of the excess current, however, since its origin is still unknown.

The reverse leakage current (due to surface effects, for example) is expected to have a relatively slow T-dependence, as is the effect of series resistance in the forward direction.

Illumination Effects

In all cases studied to date, both conventional and drift field cells, the effect of illumination can be well represented by a pure translation of the I-V curve in the negative-I direction. This is consistent with all previous descriptions of the operation of these devices, and will not be pursued further here.

Radiation Effects

Radiation damage affects the photovoltaic response much more sensitively than the dark I-V characteristics. The first observable radiation effects can be described as a slow decay of the illuminated I-V curve back along the I-direction towards the dark I-V curve. Thus the shape of the I-V curve determines the relative damage to I_{sc} and V_{oc} (the photovoltaic short-circuit current and open circuit voltage, respectively).

At considerably larger fluxes the shape of the dark I-V curve is also changed. These changes appear in both the forward and reverse characteristics. In the sections of this report which follow we will discuss the details of these changes, and correlate the experimental results with the basic current-generating processes described above.

Experimental Results

(A) Forward Characteristics

The forward I-V curve for a conventional n/p cell is shown in Fig. 2. This curve is typical of practically all of the conventional cells that we have examined. The current-voltage dependence is practically a perfect exponential function: $I = I_o [\exp(qV/nkT)]$ where n=1.6 for the cell shown.

The forward I-V for a typical sample of the early model drift field cells is shown in Fig. 3. The striking feature of this characteristic is the presence of "structure" in the characteristic, namely a current at low and moderate forward bias which is large compared with the thermal current, and which has a slower voltage dependence than the thermal current. This current dominates the forward characteristics for forward biases up to 0.5 volt, and forward currents up to 10 milliamperes. The result, as far as the operation of the drift field cells is concerned, is a distinctly un-square I-V characteristic, with a consequent loss of conversion efficiency. Also, under irradiation as the I-V curve shifts towards smaller current, there is an anomalously rapid deterioration of the photovoltage compared with the deterioration of the photocurrent.

The I-V of recent drift field cells is typified by Fig. 4. These cells are similar to conventional n/p cells as shown in Fig. 2, in that the excess current is either quite small or is totally absent.

A comparison of the room temperature and low temperature behavior of a conventional cell is shown in Fig. 5. This figure also shows the curves after irradiation with 3 MeV protons (to a flux of 10^{13} protons/cm^2). As expected, the thermal current is totally unobservable at low temperature; the current remaining at low temperature has a slow voltage dependence, and the size of the current at low bias is very nearly equal to that at room temperature. On the assumption that the departure of the room temperature I-V characteristic from pure exponential

at low voltages is the so-called excess current, we would conclude that the excess current has a small or vanishing temperature dependence.

After heavy proton irradiation the forwade I-V at room temperature is changed in a way that is best described as a large increase in the series resistance of the cell. The current at large forward bias departs markedly from the thermal (exponential) current, as shown in Fig. 5.

The residual forward current at low temperature (which we believe may be solely the excess current) is strongly affected by proton irradiation: 10^{13} protons/cm^2 produces a factor of 20 reduction in the current. Forward I-V measurements made on electron-irradiated conventional and drift field cells (with much lower effective fluxes) indicates that this effect is present under electron irradiation also: a bombardment with 2×10^{15} electrons/cm^2 @ 1 MeV produces a small relative reduction in the amount of excess current present.

Fig. 6 shows the forward characteristics for a conventional cell before and after 1 MeV electron irradiation (2×10^{15} cm^{-2}) and Fig. 7 shows the same curves for a drift field cell. There appears to be a small increase in the thermal current in both cases following irradiation, and a similarly small decrease in the excess current. Both of these changes are too small to be asserted confidently, but if real they are quite significant, and it is our recommendation that similar measurements be made on cells more heavily irradiated.

(B) Reverse Characteristics

The reverse I-V of a conventional cell at room temperature and at 77°K are shown in Fig. 8. At room temperature the current is linear with voltage. At low temperature the curve is not a pure power law, and at all voltages the dependence is faster than linear.

Similar measurements made on a drift field cell are shown in Fig. 9. In this case the temperature dependence is greater than in the conventional cell, but the general characteristics described above obtain here also. The room temperature current is linear with voltage, and the low temperature current rises faster than linearly.

The effect of proton irradiation on a conventional cell is shown in Fig. 10. Before irradiation the current is linear with voltage; after irradiation it is roughly proportional to $V^{\frac{1}{2}}$.

An electron-irradiated conventional cell is shown in Fig. 11. In this case a relatively light electron bombardment produces a definite reduction in the reverse current, but leaves its voltage dependence unchanged. In both cases the current is nearly linear with voltage.

Similar results for a drift field cell before and after electron irradiation are shown in Fig. 12. In this case irradiation reduces the reverse current sharply, but it leaves the current-voltage dependence nearly unchanged.

The temperature dependence in a lightly-irradiated drift field cell is shown in Fig. 13. The effect of cooling is similar to the effect of irradiation shown in Fig. 12; the current is reduced but the voltage dependence is unchanged.

Discussion and Conclusions

Comparing the results of measurements made on conventional solar cells and on early and recent drift field cells, we believe that the reported anomalous drop in open circuit voltage in drift field cells can be attributed completely to the excess current which is present in the early drift field cells. Since the recent drift field cells do not exhibit this current nearly to the extent seen in the early drift field cells, we believe that the phenomenon is associated with the early fabrication procedures, and that it is not inherent in the drift field configuration.

The linear current-voltage relationship which we have seen in both conventional and drift field cells is inconsistent with either generation-recombination currents or with diffusion current from the base. In the former case the current should vary as V^n where n is between 1/3 and 1/2. In the latter case, the reverse current should saturate as the reverse bias is increased. The voltage dependence of the reverse current is also inconsistent with both of these currents. The nature of the excess current and the reverse current is not known at present.

III. SPECTRAL RESPONSE

The spectral response of conventional solar cells has been calculated by Dale and Smith[2] and by Wysocki and Loferski[3]. Based on a solution of the transport equation with appropriate boundary conditions, the spectral response can be divided up into two contributions: one from the base and one from the surface layer. The base response contributes more than the surface to the overall performance of the device, and it is more easily amenable to analysis in terms of the basic properties of the base material.

Following the notation of Reference (3) the base response is given by

$$Q_B(\alpha) = \alpha L_B e^{-\alpha l} / (1 + \alpha L_B) \qquad (2)$$

where α = absorption constant, L_B = the minority carrier diffusion length in the base, l = the thickness of the surface layer. In this expression the surface reflectivity is taken to be zero.

If we consider only the wavelength region for which α is small compared with $1/l$ (l is typically less than 1 micron, so α must be smaller than 10^4 cm^{-1}) we obtain

$$Q(\alpha)/\alpha \cong \frac{1}{\alpha + 1/L_B} \qquad (3)$$

The limiting value of $Q(\alpha)/\alpha$ as α tends to zero is just L_B.

At intermediate values of α the left hand side of equation (3) approaches a $1/\alpha$ dependence. At large values of α the factor $e^{-\alpha l}$ must also be included. What is observed, in fact, is a deviation of $Q(\alpha)/\alpha$ from a purely $1/\alpha$ dependence as α increases, and this deviation may be used to determine the thickness of the surface layer.

Since the major differences (if any) between conventional and drift field cells will lie in their respective base response,

we have concentrated in the present investigation on the base response exclusively.

The expression given above for conventional cells was calculated by solving the transport equation and was based on diffusion of the minority carriers from their point of generation to the plane of the junction. To a good approximation the probability that a carrier will survive to diffuse through any distance x is a simple exponential function of x: Probability = $\exp(-x/L_B)$. As Fang has shown[4] the function $Q(\alpha)/\alpha$ is related to the Laplace transform of the collection probability function. The Laplace transform of $\exp(-x/L_B)$ is $1/(\alpha + \frac{1}{L_B})$ and this result is identical to the expression given above (Eq. 3) based on Reference 3.

In the spectral response analysis which follows, we have plotted the function $Q(\alpha)/\alpha$ vs. α in all cases. This allows a convenient, straightforward determination of the basic properties of the material before and after irradiation. In each case the response before and after electron irradiation is shown; the bombarding energy was 1 MeV and the total flux was 10^{16} electrons/cm^2 in each case.

Fig. 14 shows a typical such plot for a conventional cell. As expected, the curves saturate at low values of α and tend to go as $1/\alpha$ at higher values of α (still less than 10^4 cm^{-1}). From the saturation value of $Q(\alpha)/\alpha$ we can infer the diffusion length L_B. For the cell shown, we find that L_B(pre-irradiation) is 90 microns, and L_B(post-irradiation) is 10 microns. Writing the effect of irradiation on diffusion length in the usual form

$$\frac{1}{L^2_{B_{FINAL}}} = \frac{1}{L^2_{B\ INITIAL}} + K\phi \qquad (4)$$

we calculate that $K = 1.0 \times 10^{-10}$, a value that is in reasonable agreement with existing data on conventional cells.[5]

The shape of the spectral response of drift field cells has not previously been calculated. Following Fang's Laplace transform approach we can calculate the response for cases where the collection probability function G(x) is pure exponential.

If $G(x) = \exp(-x/L)$ in the drift field region, and $G(x) = 0$ elsewhere,

$$M(\alpha) = \int G(x)\, e^{-\alpha x}\, dx$$

$$= \int_0^w e^{-x/L}\, e^{-\alpha x}\, dx$$

$$= \frac{1}{1/L + \alpha}\left[1 - e^{-\left(\frac{1}{L} + \alpha\right)w}\right] \qquad (5)$$

The asymptotic behavior of this expression is useful in analyzing the experimental data:

At small values of α : $M(\alpha) \rightarrow L(1 - e^{-w/L})$ (6)

At large values of α : $M(\alpha) \rightarrow 1/\alpha$ (7)

We may now consider two limiting cases: (a) $L \ll w$; (b) $L \gg w$.

(a) $L \ll w$

In this case the asymptotic behavior of $M(\alpha)$ is the following:

α small:	$M(\alpha) \rightarrow L$	(8)
α large:	$M(\alpha) \rightarrow 1/\alpha$	

This result is identical to that previously described for the conventional solar cell.

(b) $L \gg w$

From Eqs. (6) and (7) the asymptotic behavior is:

α small:	$M(\alpha) \rightarrow L(1 - 1 + w/L \ldots) = w$	(9)
α large:	$M(\alpha) \rightarrow 1/\alpha$	

It is apparent from these results that it is impossible to differentiate between case (a) and case (b) from an analysis of the limiting behavior of $M(\alpha)$. Since this ambiguity exists, and since the "diffusion length" in the drift field region is

not the same as the true minority carrier diffusion length in the epitaxial material, we will hereafter refer to the experimental parameter determined from the limiting value of $M(\alpha)$ as $\alpha \to 0$ as the "depth parameter" in drift field cells.

The depth parameter in either case (a) or case (b), or in any intermediate case, cannot exceed w. Furthermore, the pre-irradiation value of the depth parameter establishes a lower limit for w, and any changes produced by irradiation must be related to a true reduction of the "diffusion length" rather than to any reduction in w. As a result, the post-irradiation value of the depth parameter can be related to the damage constant K given in Eq. (4).

Figs. 15 through 24 show $Q(\alpha)/\alpha$ vs. α for a number of drift field cells before and after irradiation. The results of our analysis of these curves are given in Table I.

The most striking feature of the results is the unusually rapid deterioration of the depth parameter under irradiation. Whereas all expectations were that the electrostatic field would assist in carrier collection, and hence reduce the value of the damage constant K, in practice the damage constants in these drift field cells are considerably higher than in conventional cells. To be specific: in conventional cells, K is typically 10^{-10}. In our sampling of drift field cells, the average value of K is 4.6×10^{-10}, and the range of values is from 2×10^{-10} to 1×10^{-9}. The worst cases, TI 4-4 and TI 4-5, were a factor of 10 more damage susceptible than conventional cells.

TABLE I

Cell Number	Depth Parameter (microns) Before irradiation	Afterwards	K
TI 1A-1	14	3.5	7.8×10^{-10}
1A-2	16.2	4.1	5.4
2-1	19	6.7	2.0
2-2	19	4.5	4.7
3-4	28	6.7	2.0
3-5	30	6.7	2.0
3-6	32	7.8	1.7
4-4	12	2.8	10.
4-5	10	2.8	10.
5-1	33	5.6	3.0
5-2	37	7.0	1.9

CONCLUSIONS AND RECOMMENDATIONS

To summarize our findings to date:

(1) The excess current which we have observed in early models of the drift field cell were responsible, in our opinion, for the reported anomalous voltage degradation in these cells upon irradiation.

(2) Samples of drift field cells made in recent production do not exhibit as high an excess current as did the early drift field cells; as a result, the recent cells do not show any unusual degradation in the open circuit photovoltage under bombardment.

(3) The excess current may easily be monitored in any production run of drift field (or conventional) cells. If this is done, a relatively important factor in determining the radiation damage rate of these cells can be controlled or eliminated. It is our recommendation, therefore, that such monitoring be done, at least on a sampling basis, in future production runs.

(4) The results of our spectral response analysis indicate unambiguously that the drift field material (epitaxial silicon) has significantly higher damage susceptibility than the material used in making conventional solar cells (1-10 ohm-cm). We recommend, therefore, that if research & development in drift field cells is to be continued a more basic study of radiation damage in epitaxial silicon is almost mandatory. Such a program should consist of Hall measurements, lifetime & trapping studies, EPR, infrared absorption and photoconductivity, etc.

The work which has been done to date, including the present investigation, has not yet answered the question as to the future of the drift field solar cell. It does indicate, in our opinion, that a straightforward continuation of present programs on their present scales is not likely to be successful.

ACKNOWLEDGEMENT

The work described in this report was the result of considerable collaboration between Princeton Research & Development Co. and NASA - Goddard Space Flight Center. Dr. P. H. Fang and Y. M. Liu provided the spectral response data and portions of the I-V data used in our analysis. In addition, P. H. Fang stimulated and assisted in formulating our approach to the problem.

REFERENCES

(1). C-T Sah, R. N. Noyce, and W. Shockley, Proc. IRE 1228 (1957).

(2). B. Dale and F.P. Smith, J. Appl. Phys. 32, 1377 (1961).

(3). J.J. Wysocki and J. J. Loferski, RCA Review 22, 38 (1961).

(4). P. H. Fang, unpublished study.

(5). W. Rosenzweig, Bell Syst. Tech. J. 41, 1573 (1962); W. Rosenzweig, H. K. Gummel, and F. M. Smits, Bell Syst. Tech. J. 42, 399 (1963).

Figure 1.

Equivalent Circuit Used to Analyze Solar Cells

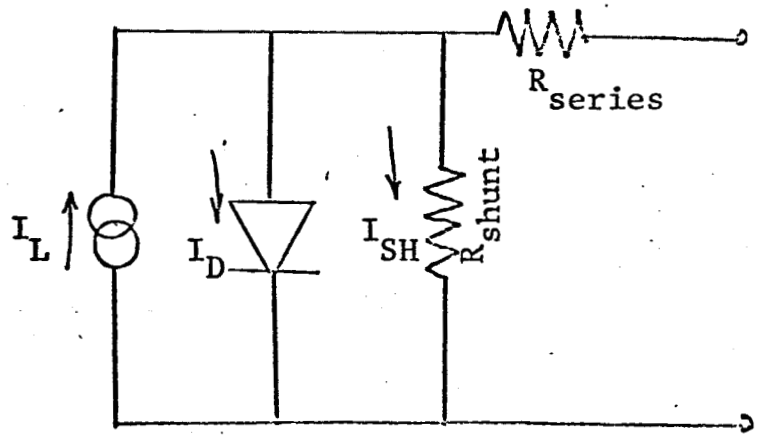

I_L = Light-generated current

I_D = Diode current

I_{SH} = Shunt current

Figure 2. Forward I-V Characteristics of a Conventional Solar Cell

Room Temperature

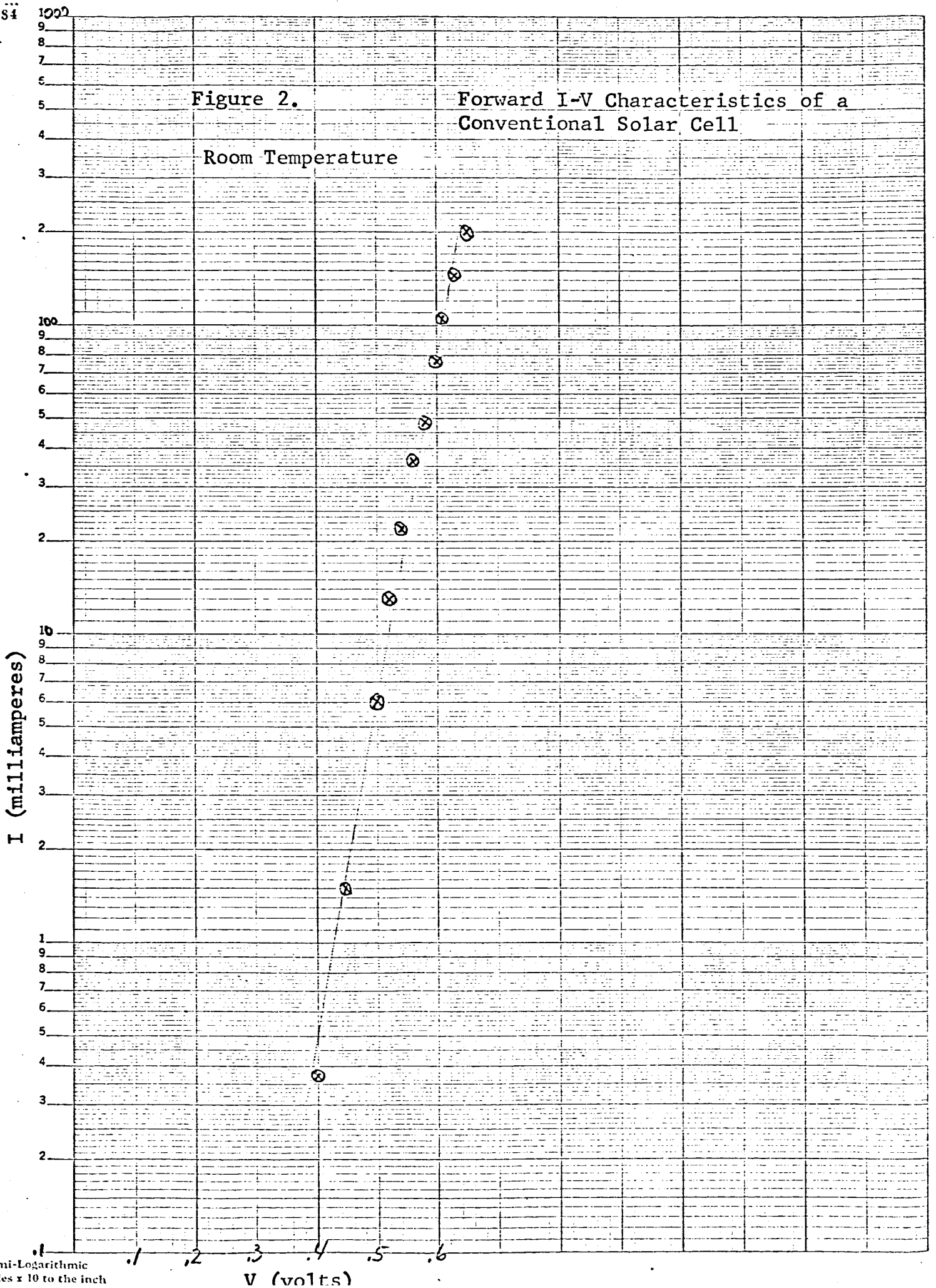

Semi-Logarithmic
4 Cycles x 10 to the inch

Figure 3. Forward I-V Characteristics of a Drift Field Cell (TI-94) Showing Thermal and Excess Currents

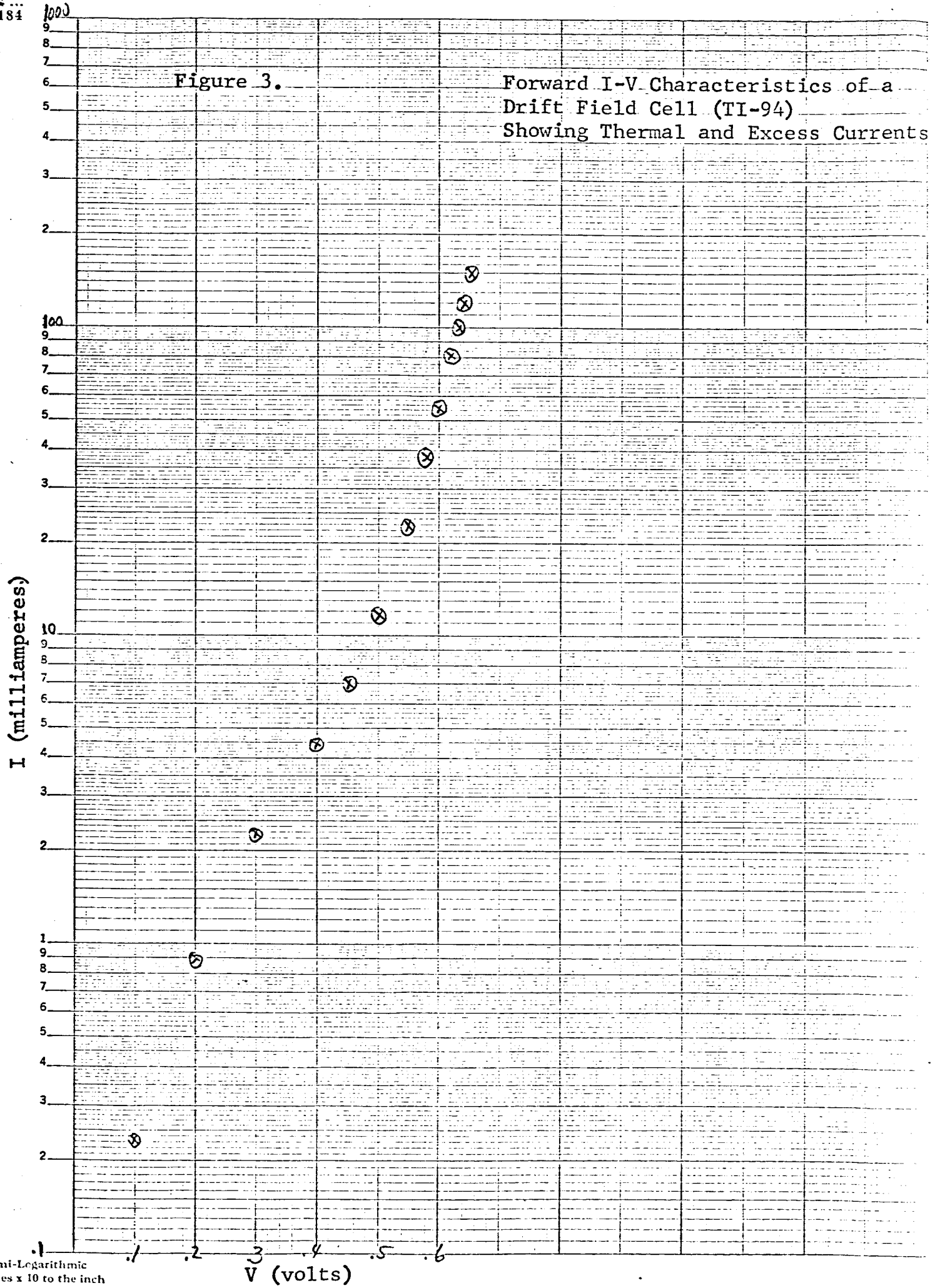

Semi-Logarithmic
4 Cycles x 10 to the inch

Figure 4. Forward I-V Characteristics of a Drift Field Cell (TI 3-9)

Room Temperature

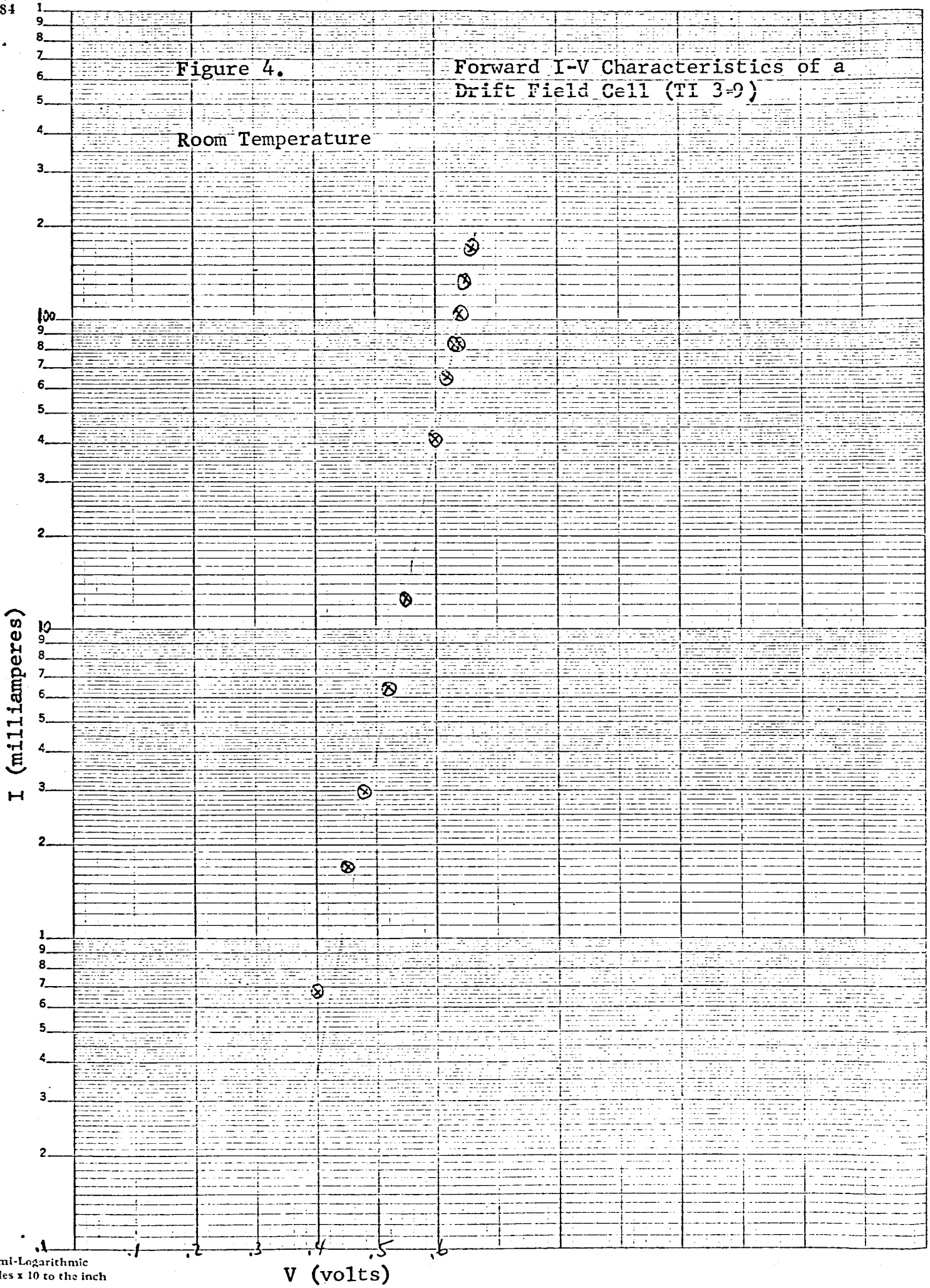

Semi-Logarithmic
4 Cycles x 10 to the inch

Figure 5.

#86

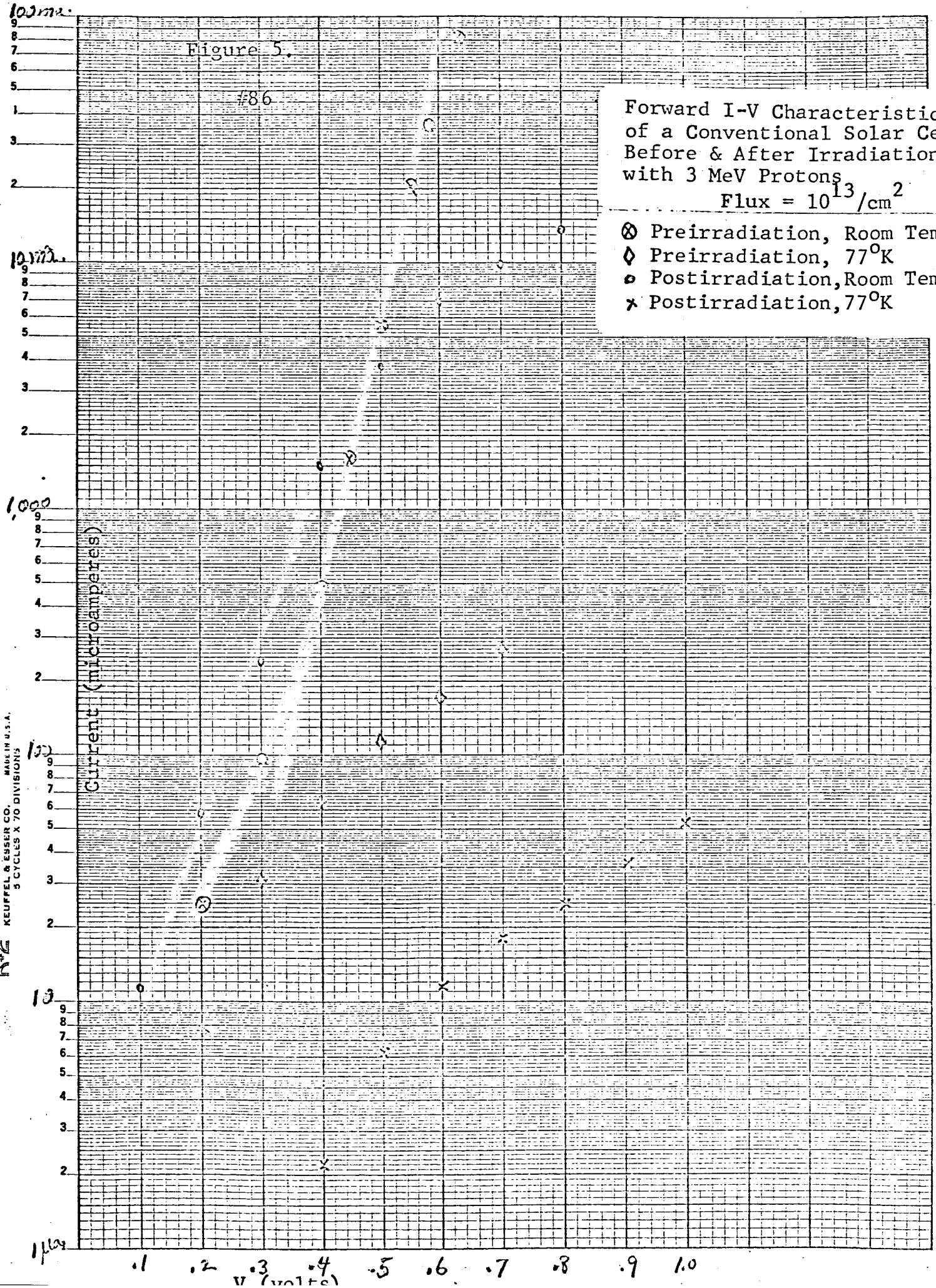
Forward I-V Characteristics of a Conventional Solar Cell Before & After Irradiation with 3 MeV Protons
Flux = $10^{13}/cm^2$
⊗ Preirradiation, Room Temp.
◊ Preirradiation, 77°K
o Postirradiation, Room Temp.
x Postirradiation, 77°K
Current (microamperes)
100ma.
10ma.
1,000
100
10
1μa
.1
.2
.3
.4
.5
.6
.7
.8
.9
1.0
V (volts)
SEMI-LOGARITHMIC 359-91
KEUFFEL & ESSER CO. MADE IN U.S.A.
5 CYCLES X 70 DIVISIONS

12-184

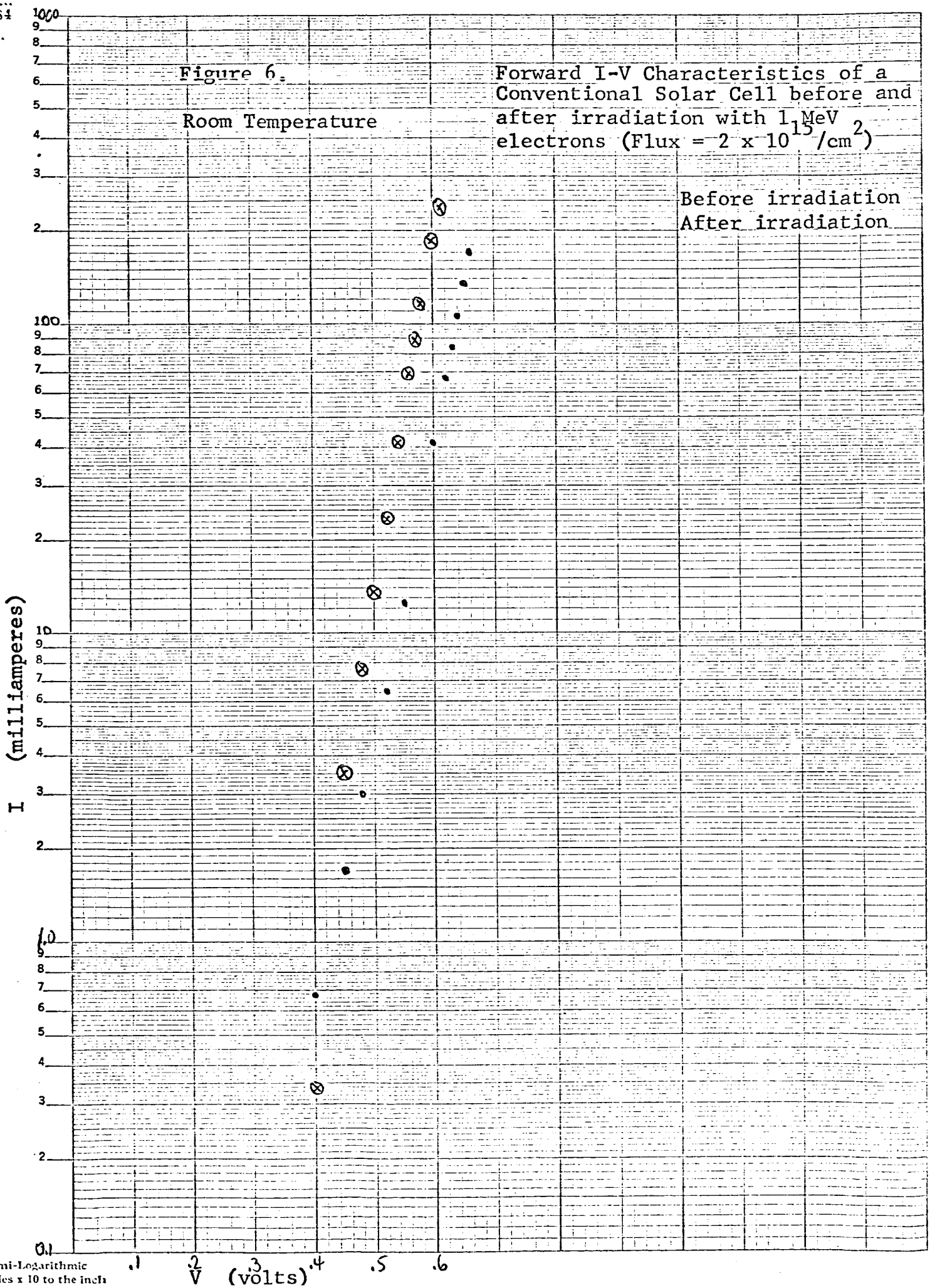

Figure 6.

Forward I-V Characteristics of a Conventional Solar Cell before and after irradiation with 1 MeV electrons (Flux = 2×10^{15} /cm^2)

Room Temperature

⊗ Before irradiation
• After irradiation

· Semi-Logarithmic
4 Cycles x 10 to the inch

Figure 7.

TI 3-8
Room Temperature

Forward I-V Characteristics of a Drift Field Cell Before and After Irradiation with 1 MeV electrons (Flux = $2 \times 10^{15}/cm^2$)

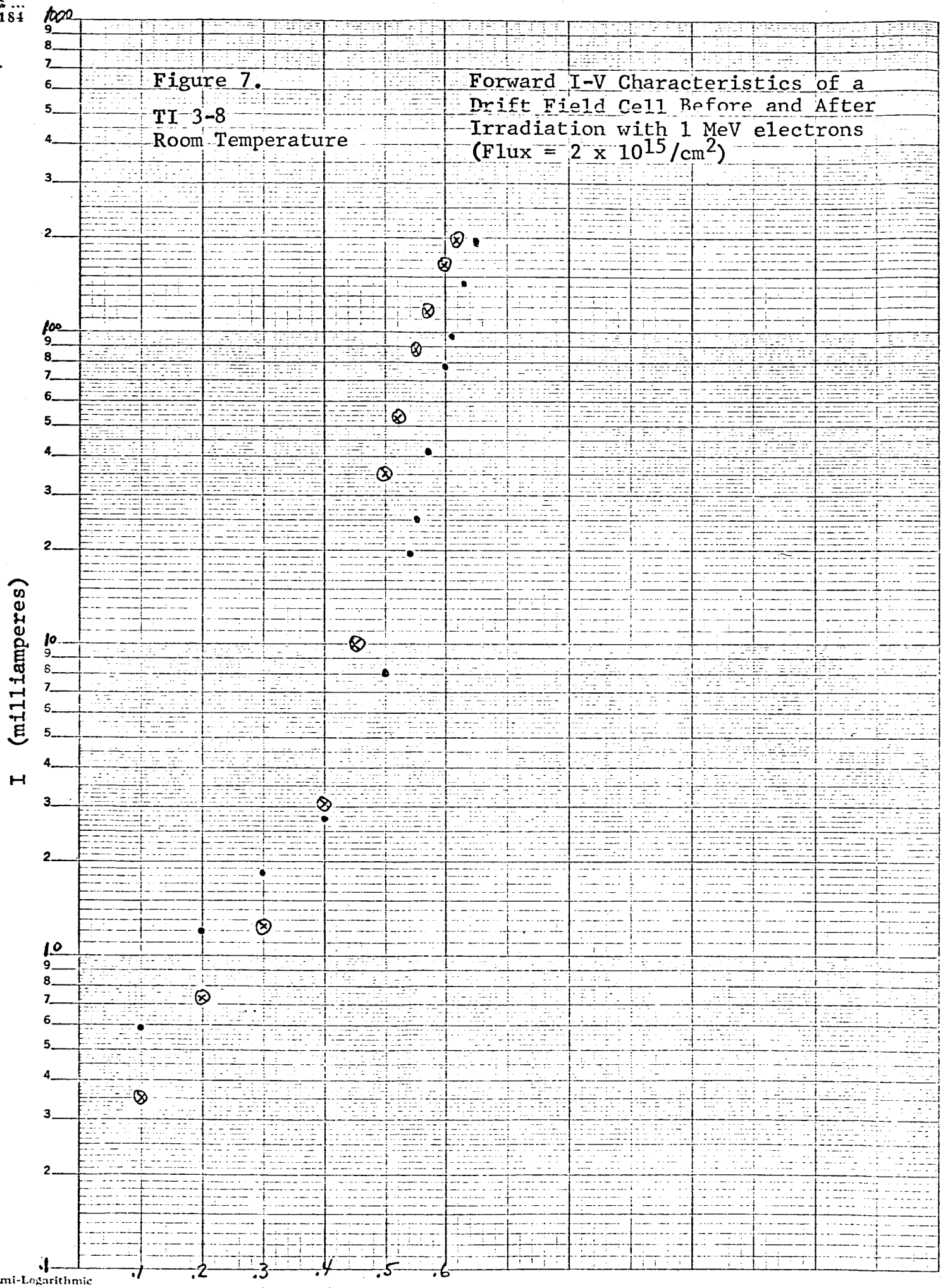

Semi-Logarithmic
4 Cycles x 10 to the inch

Figure 8.

Reverse I-V Characteristics of a Conventional Solar Cell

⊙ Room Temperature

× 77°K

Unirradiated

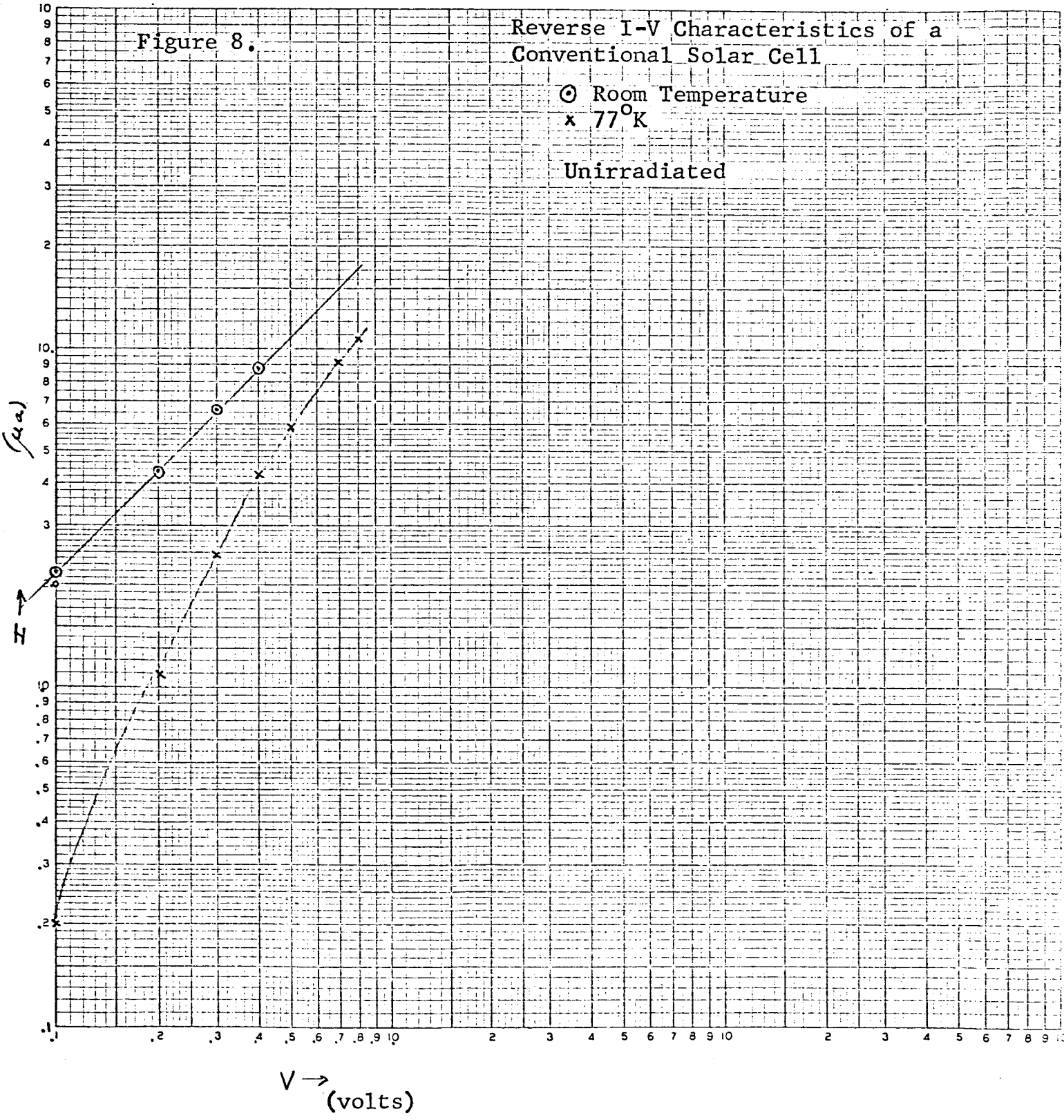

Full Logarithmic, 3 × 3 Cycles

Figure 9.

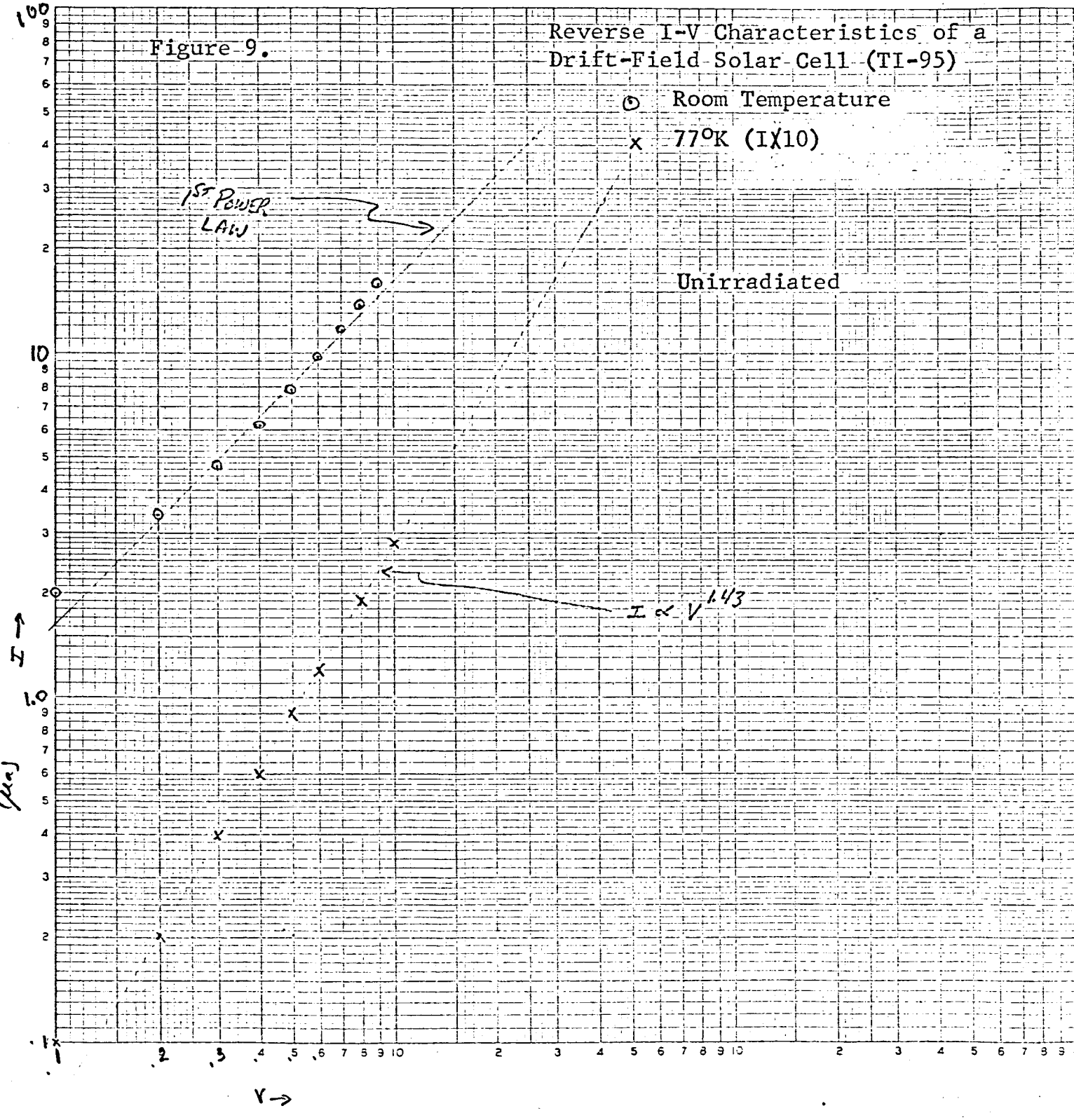

Full Logarithmic, 3 × 3 Cycles

Figure 10.

Reverse I-V Characteristics of a Conventional Solar Cell before and after Proton Irradiation

#86
Room Temperature

Before Irradiation
After 10^{13} protons/cm^2 @ 3 MeV

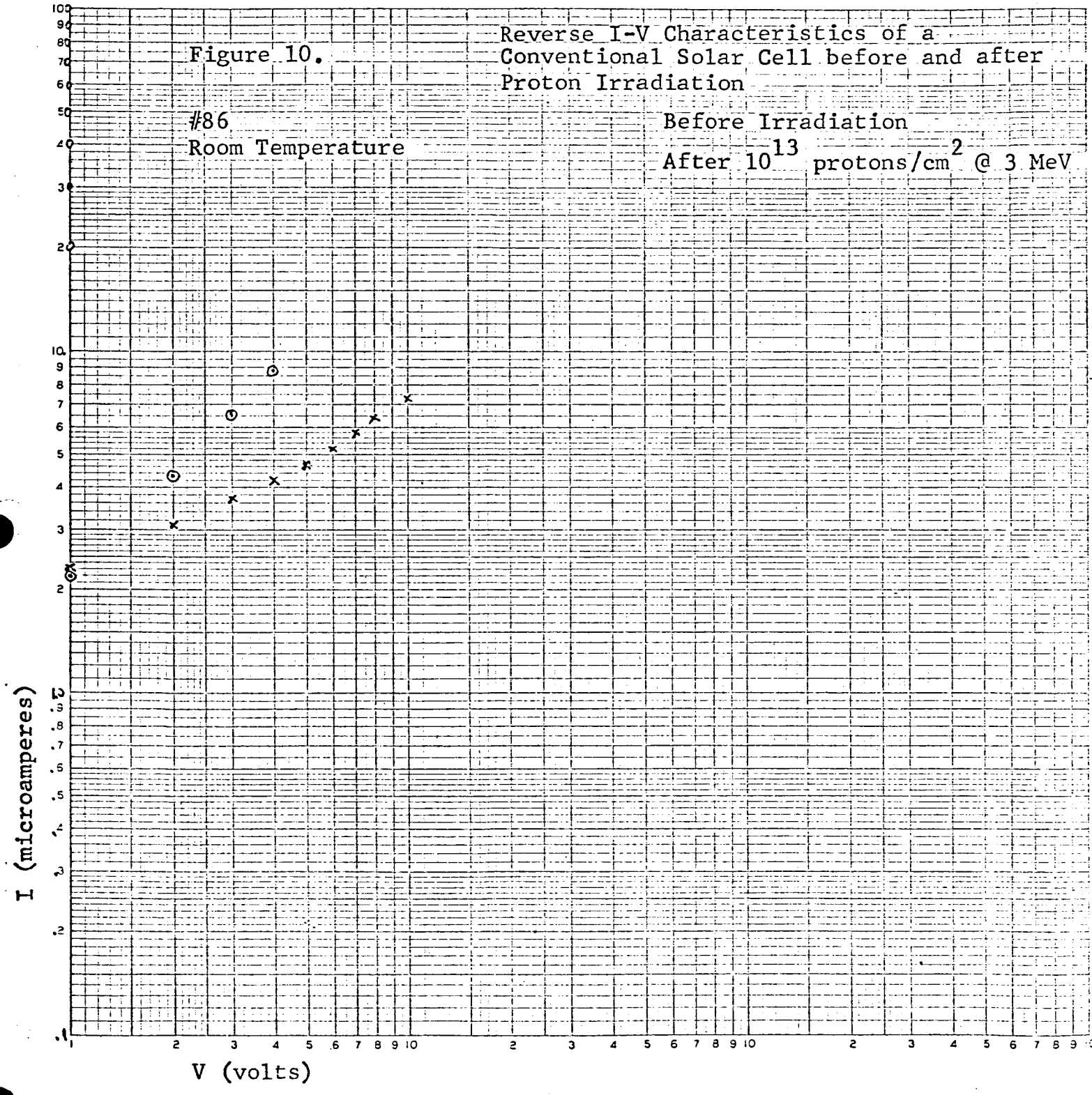

Full Logarithmic, 3 × 3 Cycles

Figure 11.

Reverse I-V Characteristics of a Conventional Solar Cell Before and After Electron Irradiation

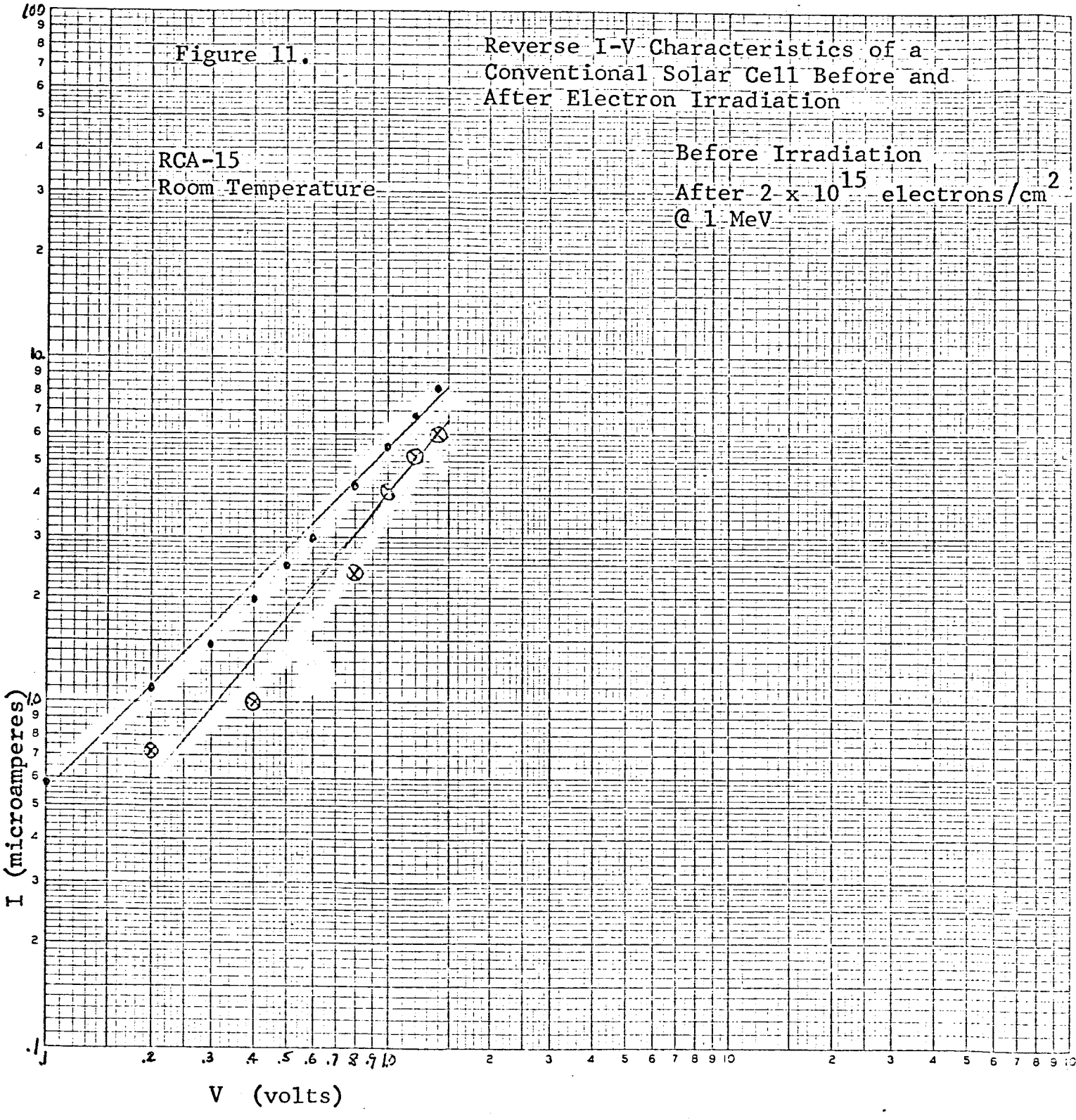

Full Logarithmic, 3 × 3 Cycles

Figure 12

TI-95

Room Temperature

Reverse I-V Characteristics of a Drift Field Solar Cell Before and After Electron Irradiation

⊡ Before Irradiation

⊗ After 10^{16} electrons/cm^2 @ 1 MeV

⊙ After 10^{17} electrons/cm^2 @ 1 MeV

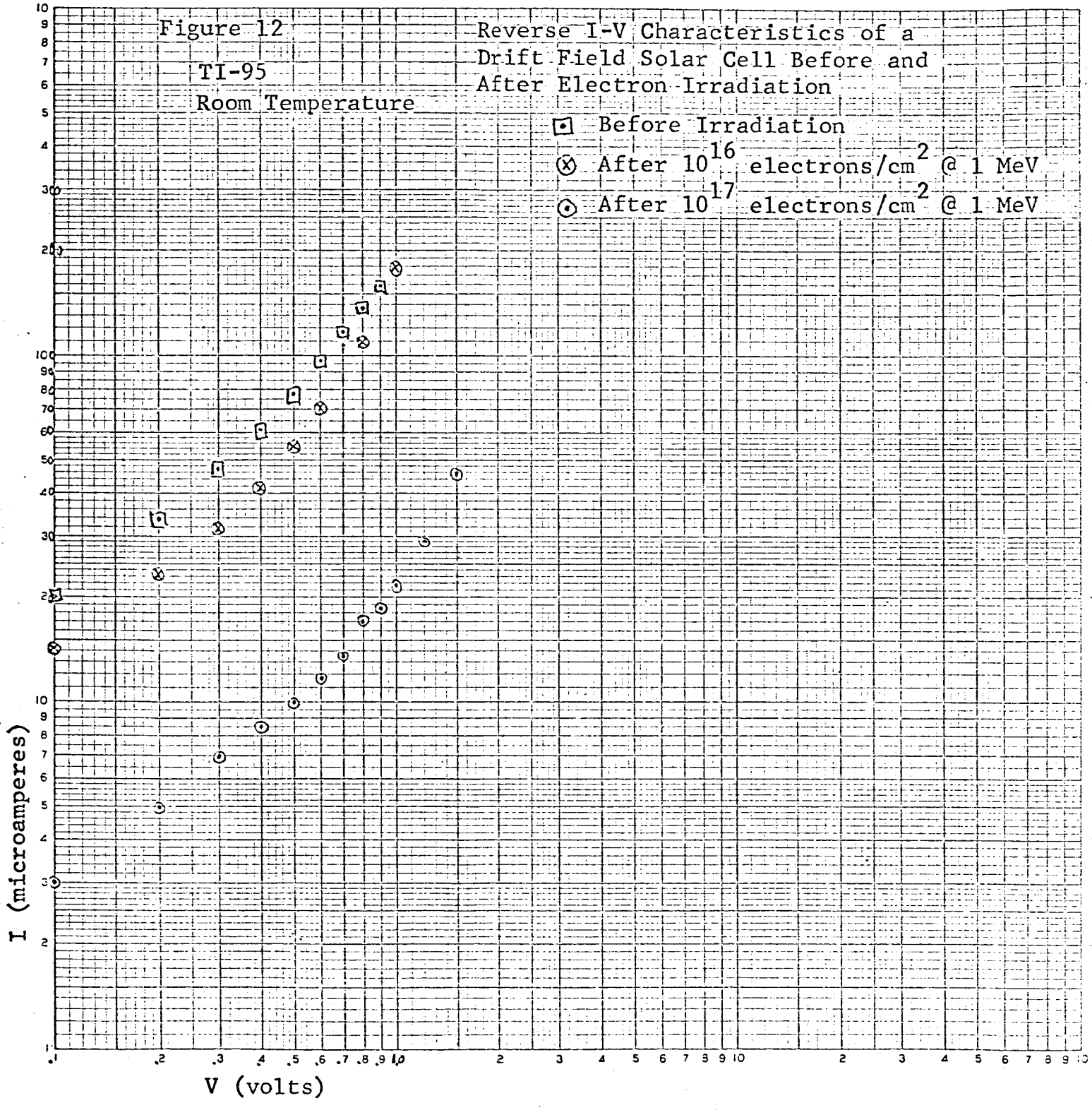

Full Logarithmic, 3 × 3 Cycles

Figure 13.

Reverse I-V Characteristics of a Drift Field Solar Cell (TI-95) Irradiated with 10^{16} electrons/cm^2 at 1 MeV.

o Room Temperature

x $77^{o}K$ (I x 10)

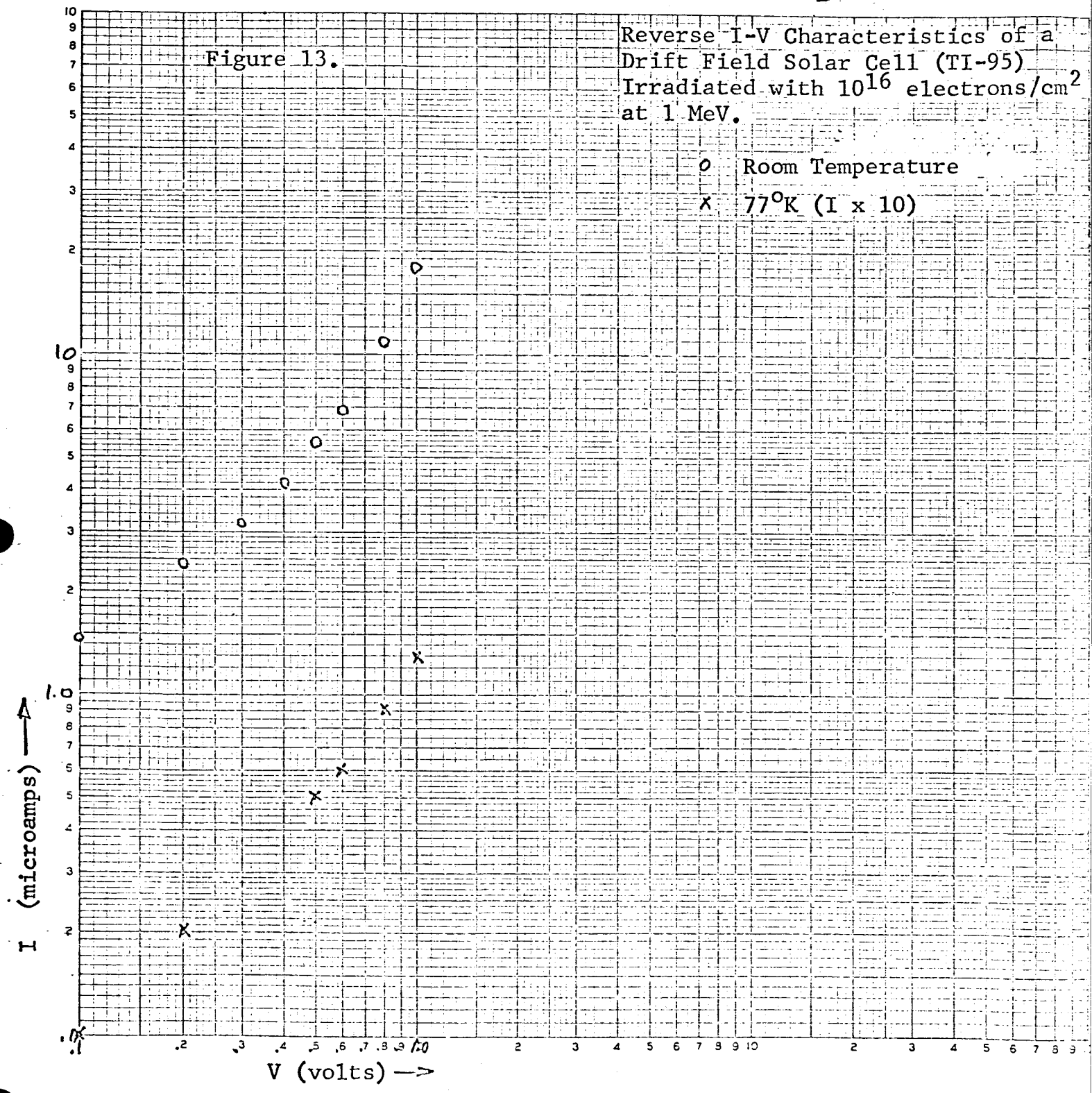

Full Logarithmic, 3 × 3 Cycles

RCA-1

Figure 14.

$Q(\alpha)/\alpha$ vs. α for a typical Conventional Cell.

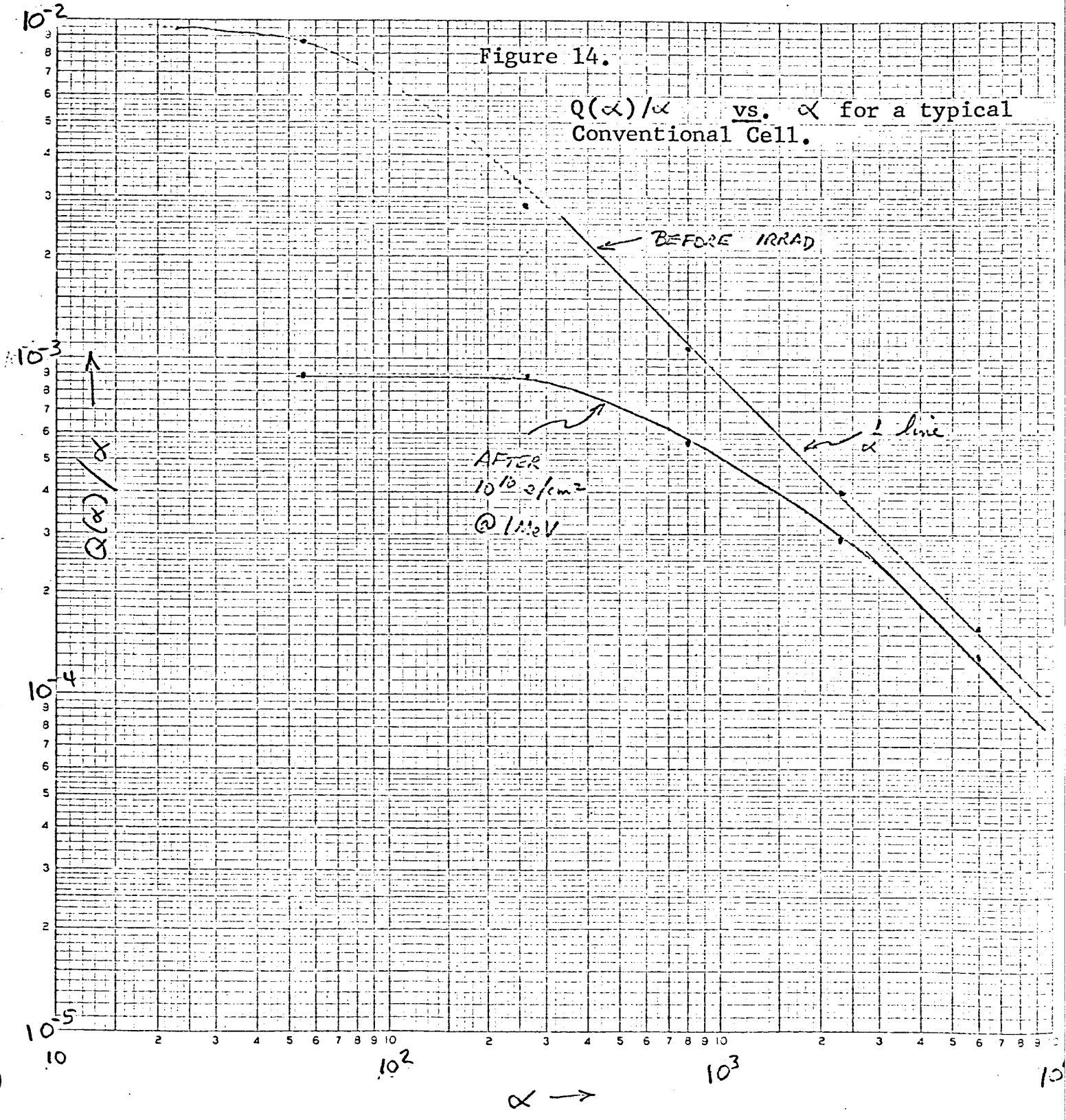

Full Logarithmic, 3 × 3 Cycles

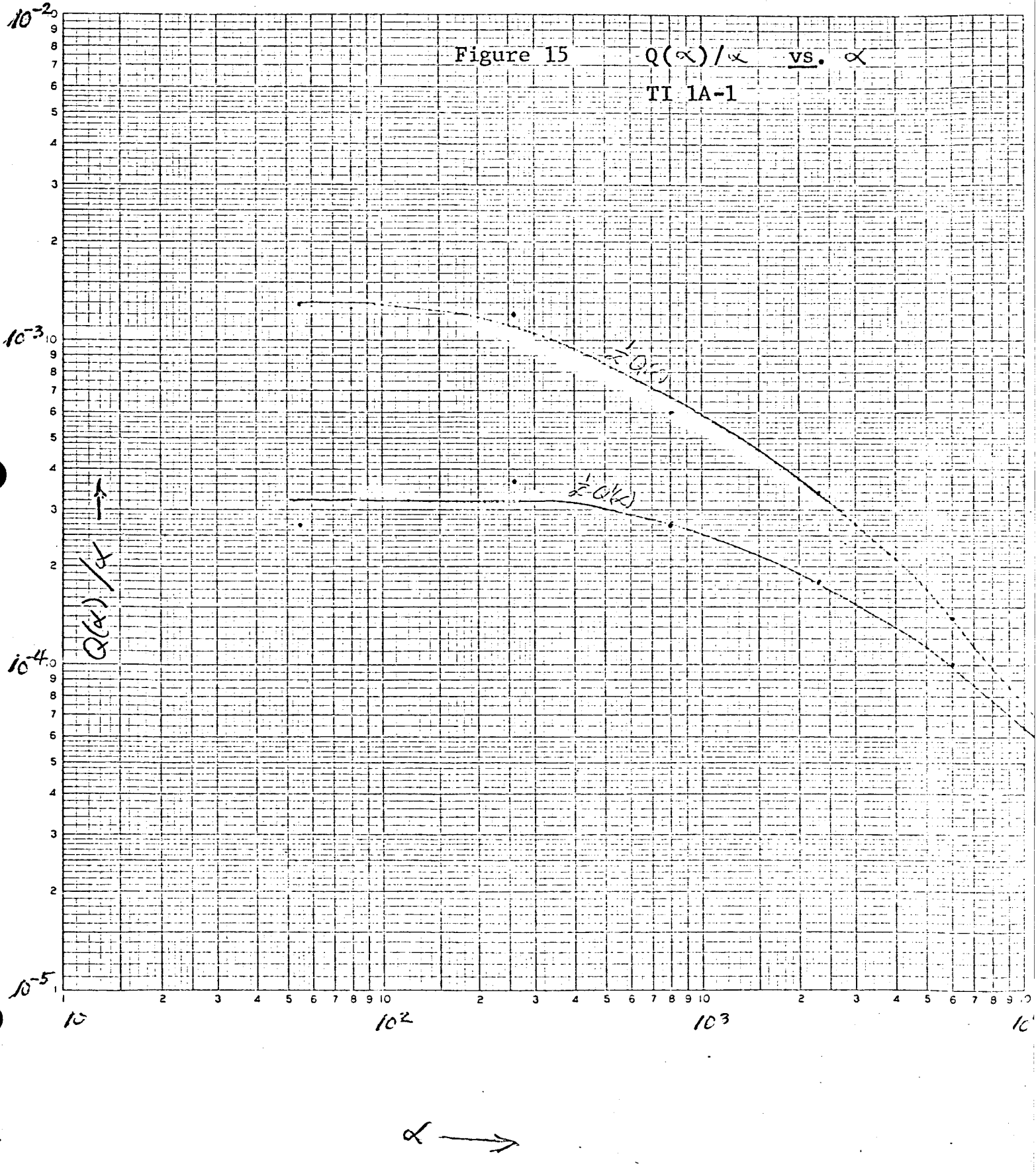

Full Logarithmic, 3 x 3 Cycles

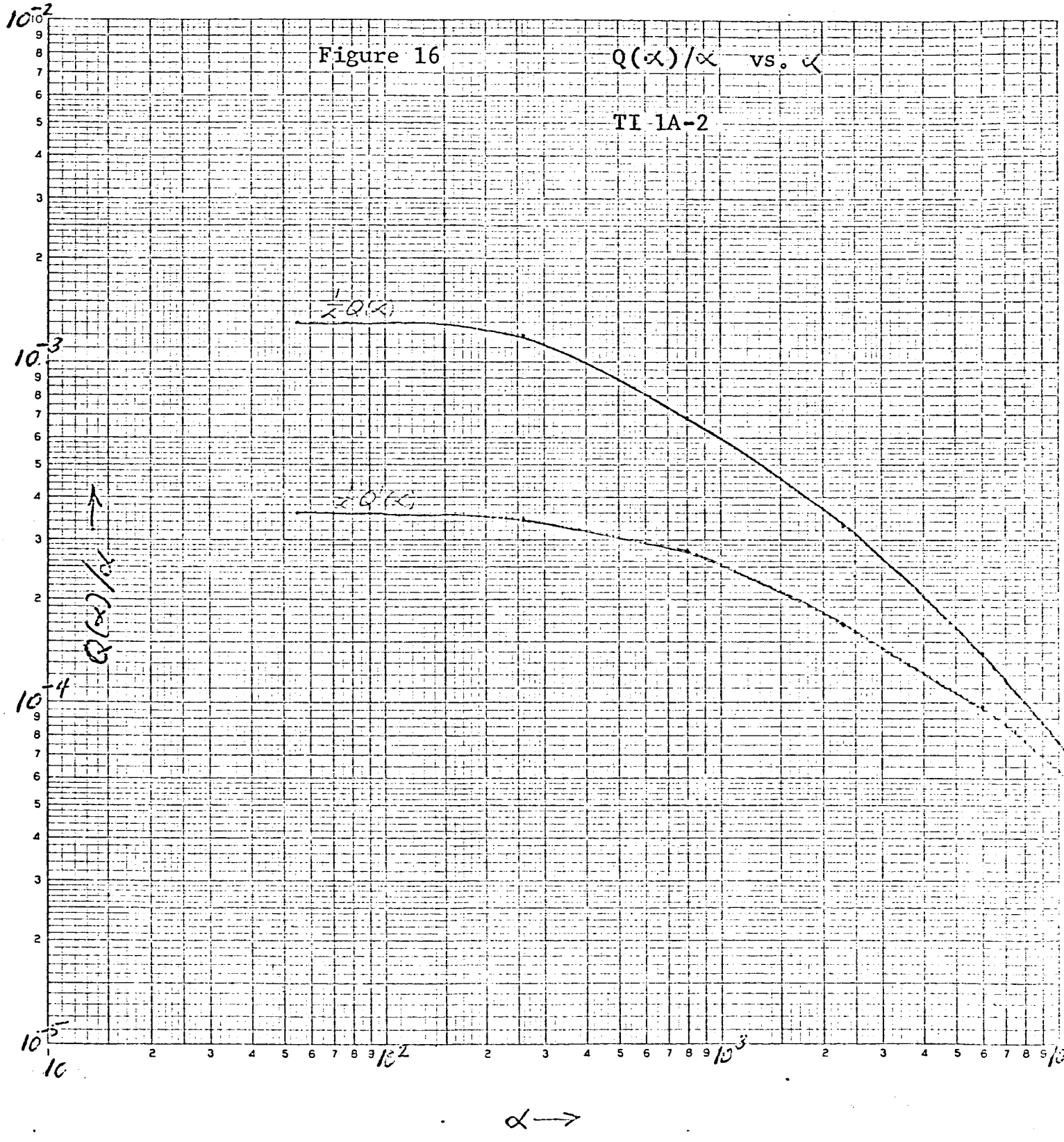
Figure 16
Q(α)/α vs. α
TI-1A-2
½Q(α)
αQ'(α)
Q(α)/α
α

Figure 17. $Q(\alpha)/\alpha$ vs. α

TI 2-1

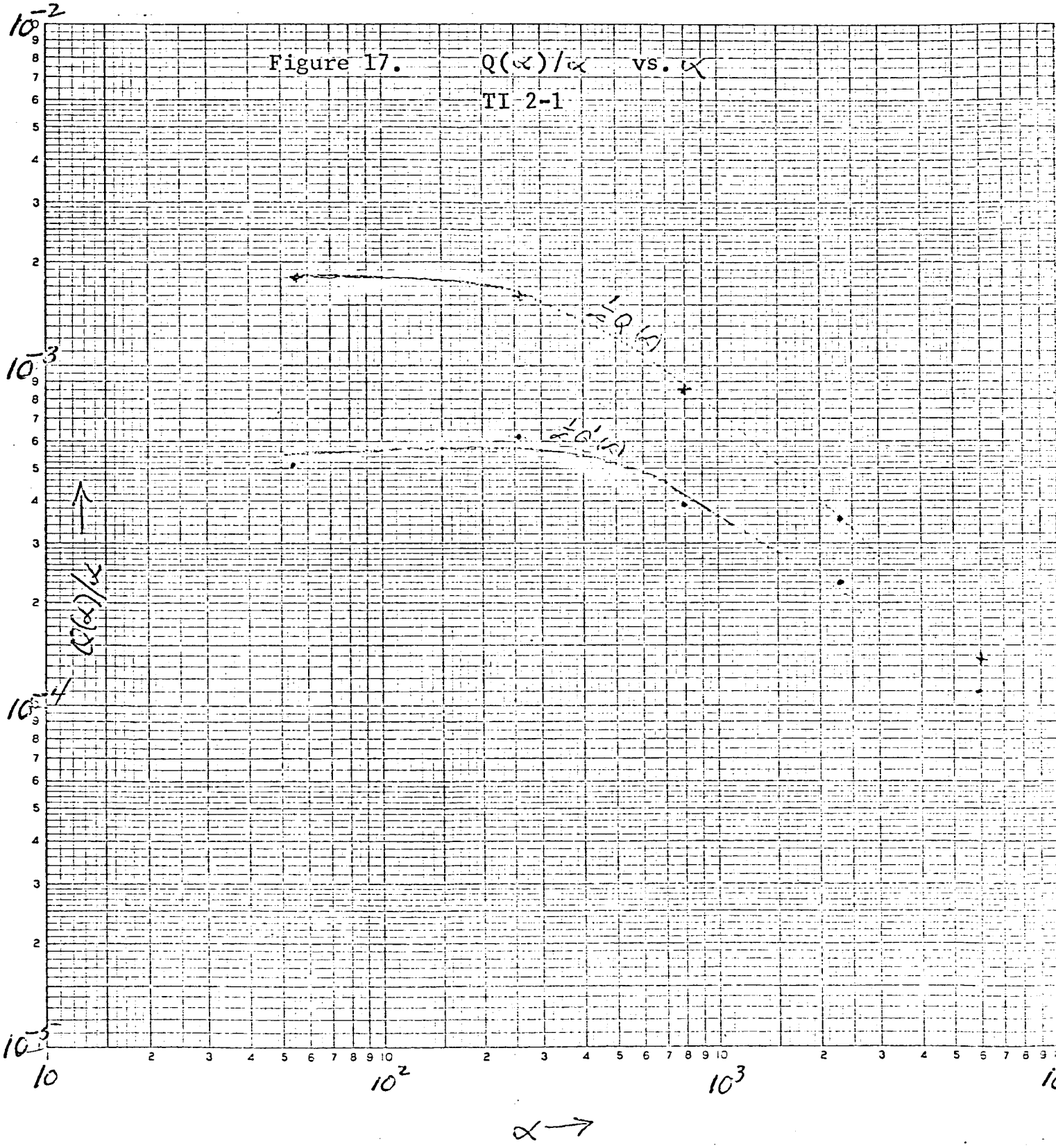

Figure 18 $Q(\alpha)/\alpha$ vs. α

TI 2-2

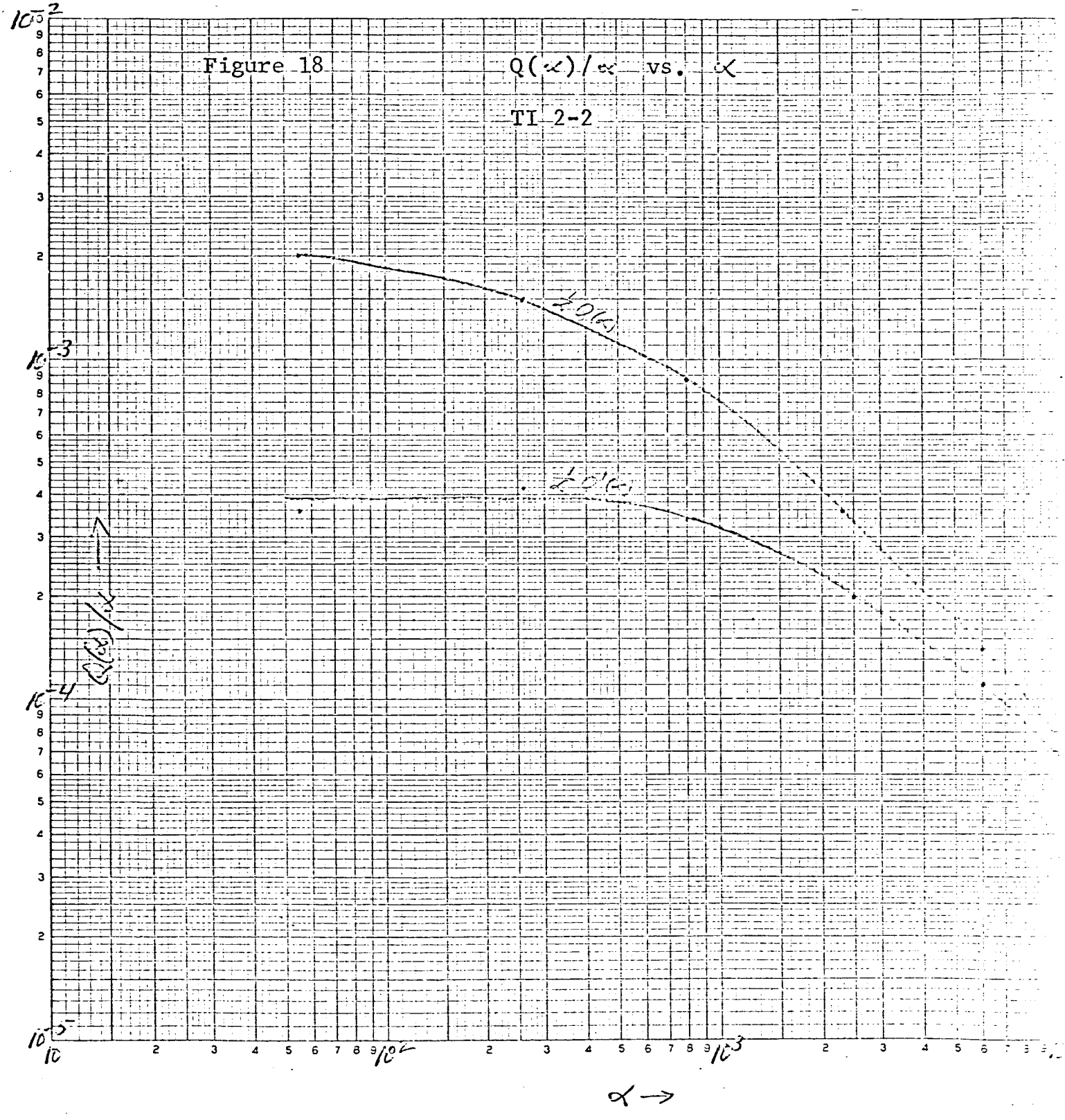

Figure 19 $Q(\alpha)/\alpha$ vs. α

TI 3-4

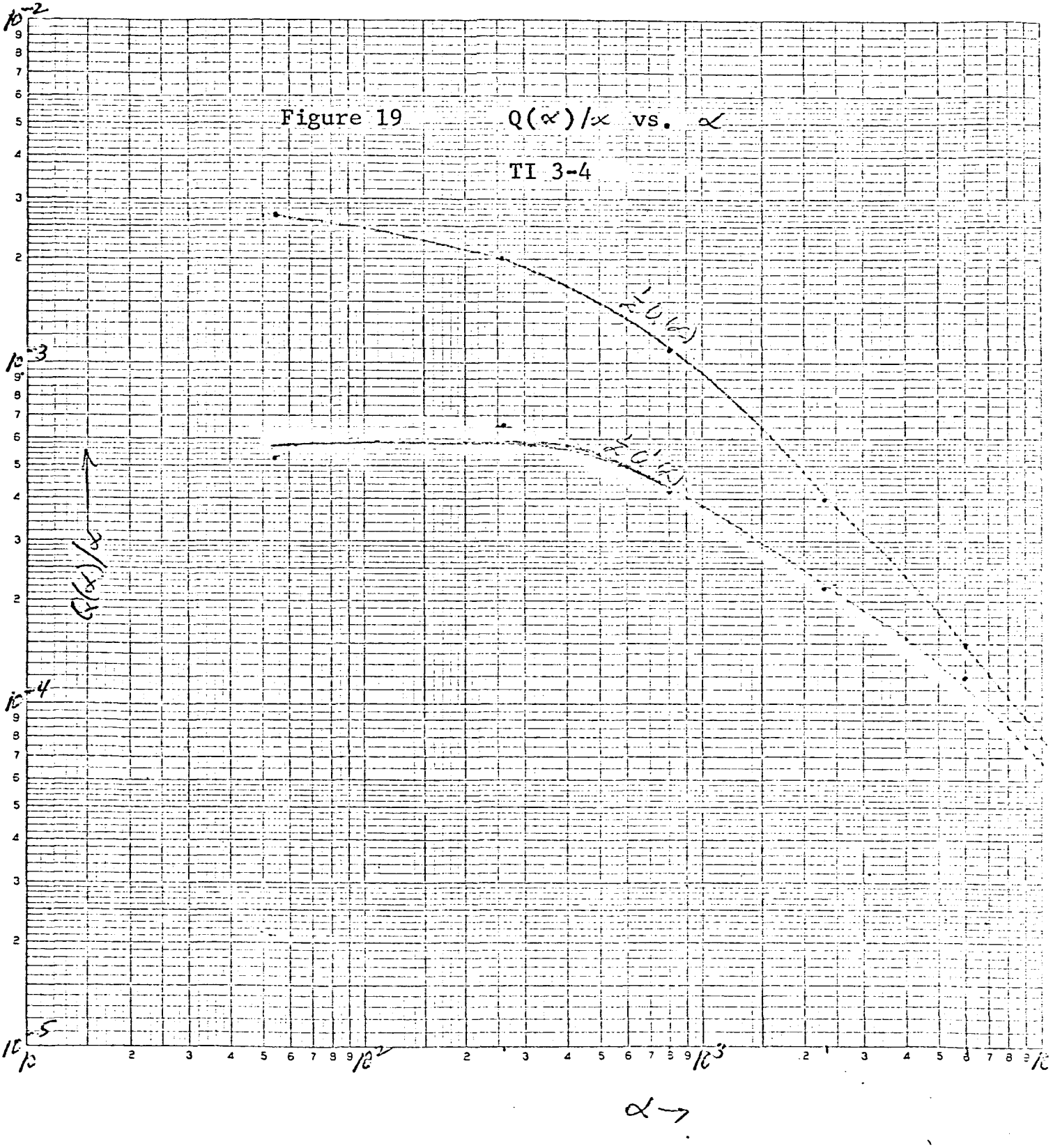

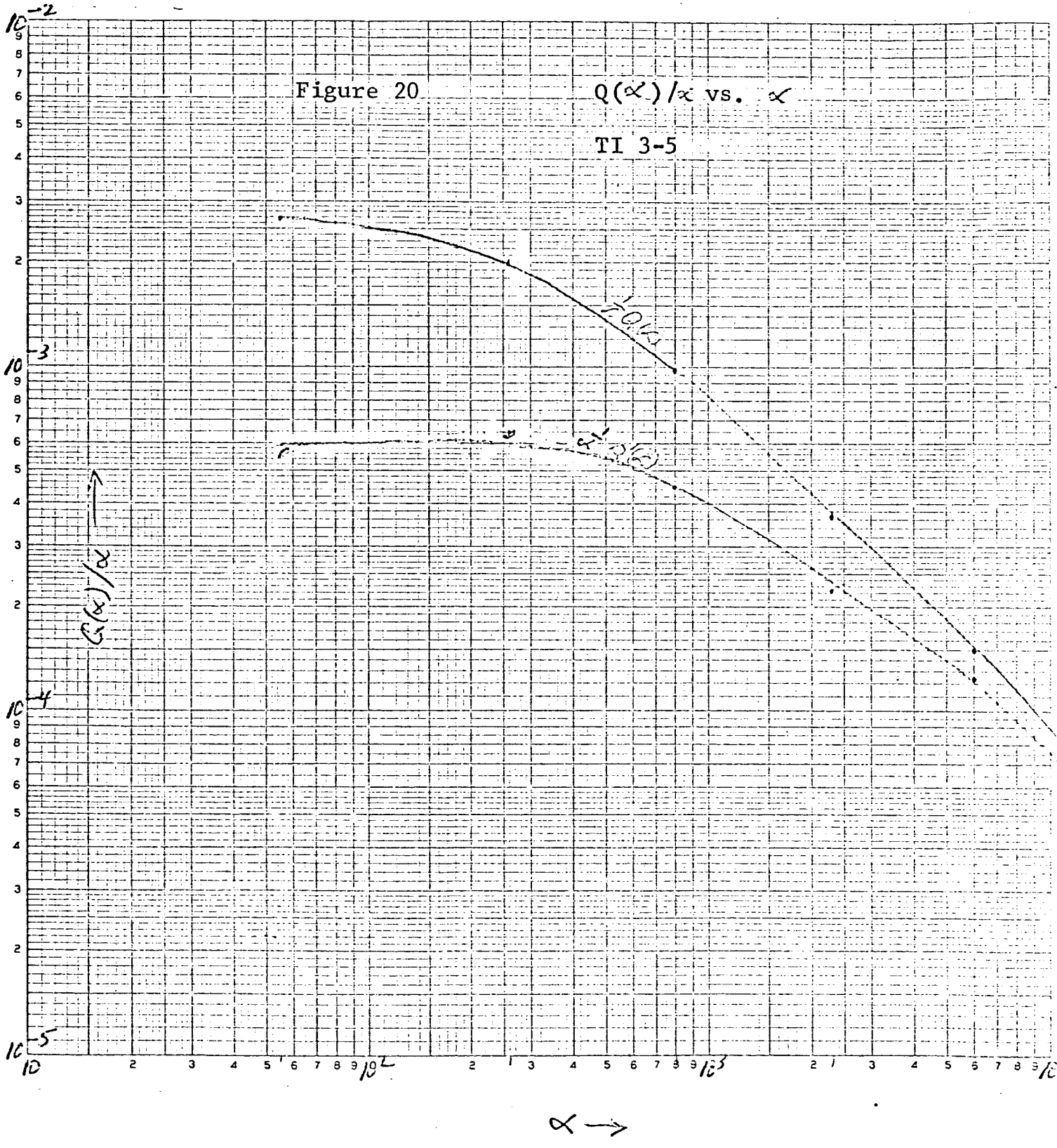
Figure 20
Q(α)/α vs. α
TI 3-5
Q(α)/α
α
α'
10^-2
10^-3
10^-4
10^-5
10^0
10^1
10^2
10^3

Figure 21 $Q(\alpha)/\alpha$ vs. α

TI 3-6

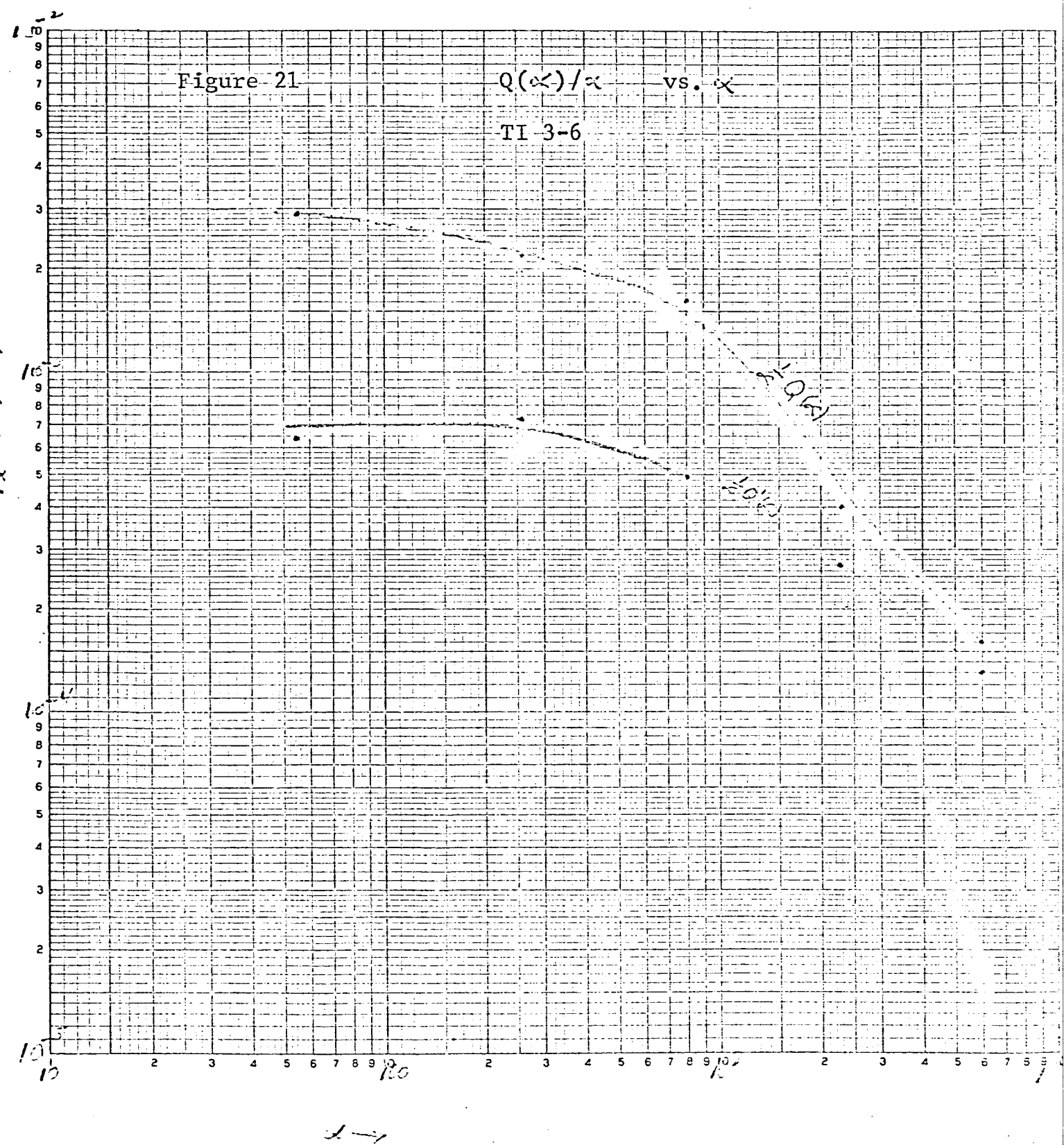

Full Logarithmic, 3 × 3 Cycles

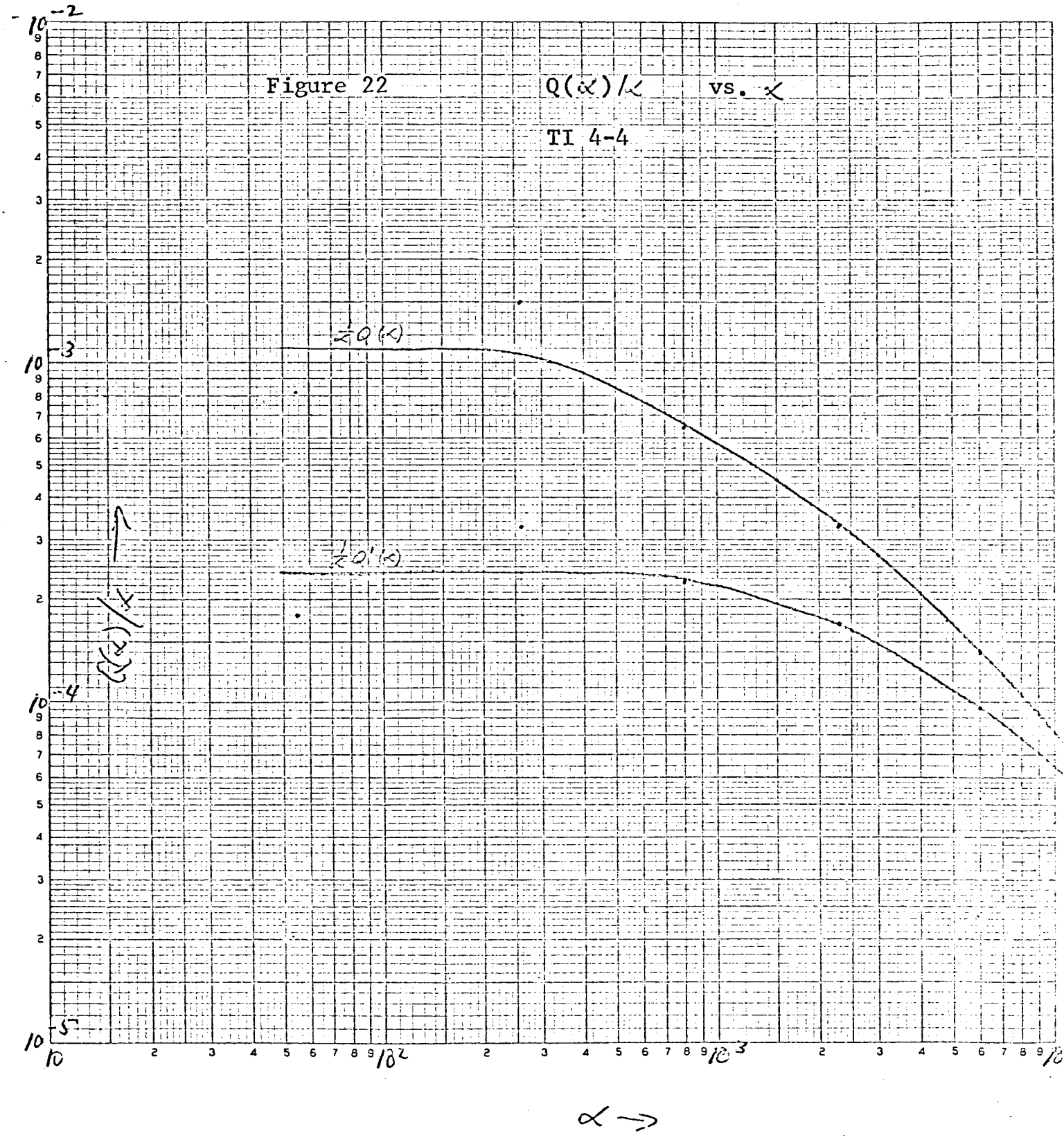

· Full Logarithmic, 3 × 3 Cycles

12-081

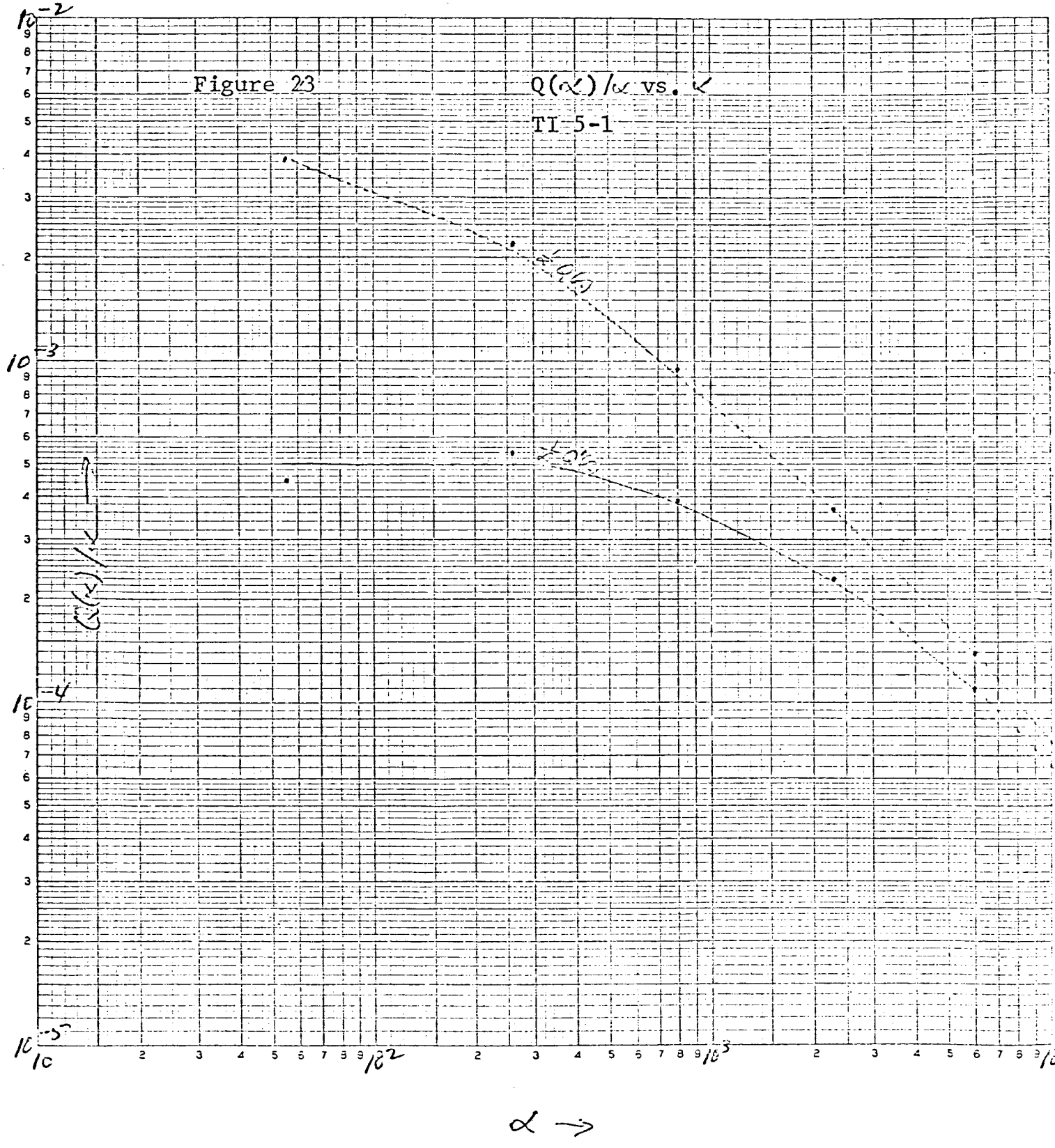

Full Logarithmic, 3 × 3 Cycles

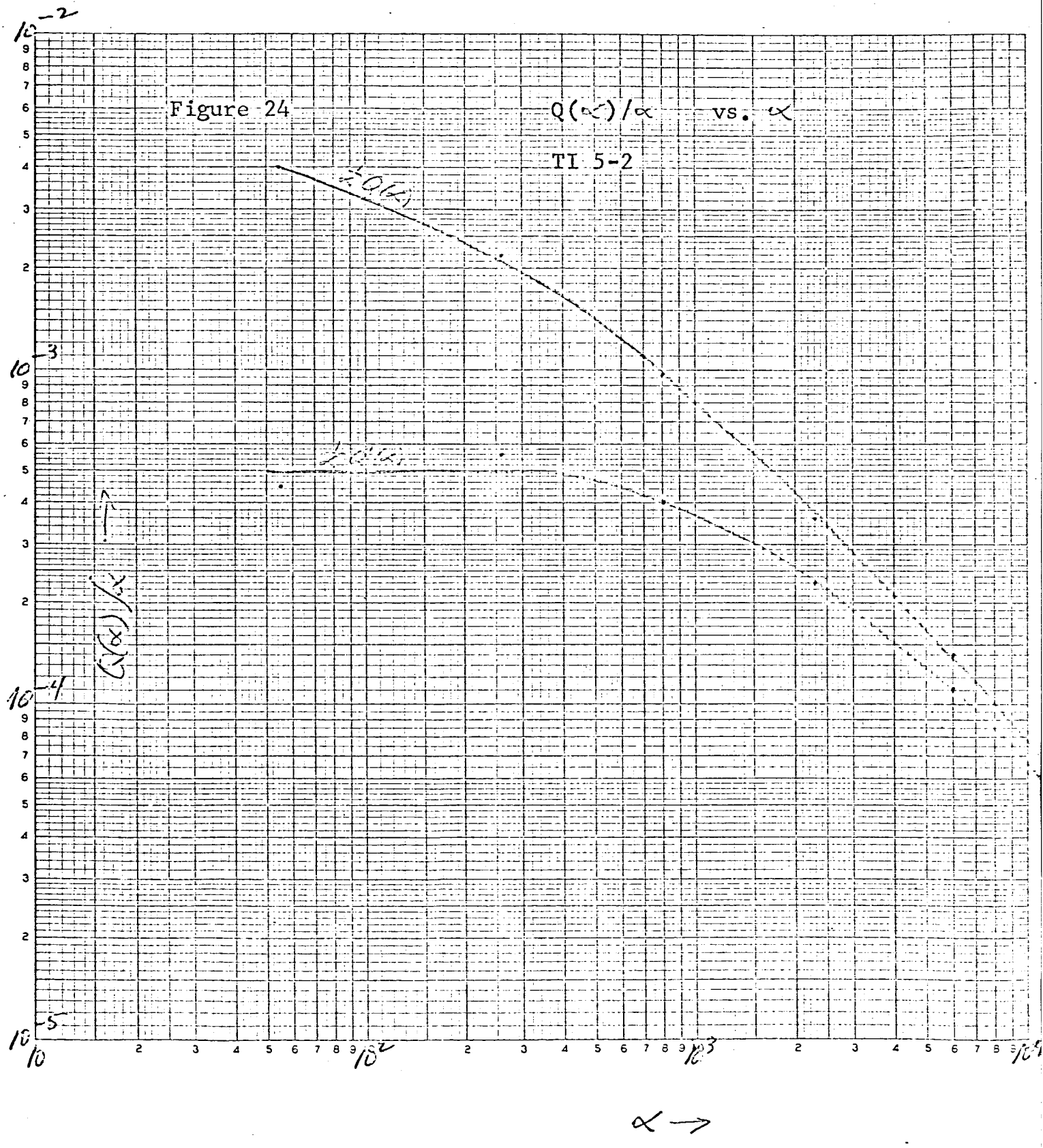
Figure 24
Q(∝)/∝ vs. ∝
TI 5-2
Q(∝)/∝
∝